Supplementary Materials and Methods

RNA extraction and quantitative real-time PCR

For RNA extraction, total RNA was extracted using Cell RNA isolation Kit (Vyzame) according to the manufacturer's guidance, and cDNA was synthesized using Reverse Transcription Kit (Vyzame) following the manufacturer's protocol.

For quantitative real-time PCR, Quantitative PCR was performed with SYBR Mixture (Vyzame) on a CFX96 Real Time PCR Detection System (Bio-Rad). β-Actin served as the internal control. Relative quantification was performed using the ΔΔCT method. The primers used in this paper were listed in Table S5.

Western Blotting and immunoprecipitation (IP)

Cells were lysed in EBC buffer (50 mM Tris pH 7.5, 120 mM NaCl, 0.5% NP-40) supplemented with protease inhibitors (Complete Mini, Roche) and phosphatase inhibitors (phosphatase inhibitor cocktail set I and II, Calbiochem). The lysates were then resolved by SDS-PAGE and immunoblotted with indicated antibodies. Protein concentrations were measured using a Beckman Coulter DU-800 spectrophotometer using the Bio-Rad protein assay reagent. Equal amounts of protein were resolved by SDS–PAGE using a standard protocol. For immunoprecipitation, 1 ml 1% NP40 lysates were incubated with the appropriate ANTI-FLAG® M2 Affinity Gel or Anti-HA MagBeads overnight at 4 °C. Immuno-complexes were washed three times with NETN buffer (20 mM Tris, pH 8.0, 100 mM NaCl, 1 mM EDTA and 0.5% NP-40) before being resolved by SDS-PAGE and immunoblotted with indicated antibodies. For endogenous co-immunoprecipitation assay, cells were lysed with NP-40 buffer (10 mM Tris-HCl, pH 7.5, 150 mM NaCl, 0.5% NP-40, protease inhibitors cocktail, 5% glycerol, 10 mM NaF, 1 mM PMSF). Whole cell lysates obtained by centrifugation were incubated with 5 mg of antibody and protein G agarose beads (Invitrogen) overnight at 4℃. The immunocomplexes were then washed with NP-40 buffer for 3 times and separated by SDS-PAGE for further western blotting assays. Antibodies used in this paper were listed in Table S1.

Cytoplasmic and Nuclear Extraction

Adherent cells at 90–100% confluence were washed twice with ice-cold PBS and lysed directly on plates using the manufacturer's cytoplasmic extraction buffer (Invent, SC-003), followed by 5 min incubation on ice and scraping to collect lysates. After vortexing, samples were centrifuged at top speed for 5 min at 4 °C to obtain the cytosolic fraction. Nuclear pellets were resuspended in nuclear extraction buffer, subjected to repeated vortex/ice cycles, and passed through the supplied filter cartridges by brief high-speed centrifugation to yield nuclear extracts.

In Vitro Cell viability assays

For cell viability assay, the cells were seeded in 96-well plates with appropriate confluences. For DOT1L inhibition, cells were pretreated with SGC0946 for 48 hours. Sixteen hours after seeding, cells were treated with indicated concentrations of ferroptosis inducers. After 6 hours of treatment, the plates were incubated with CCK-8 for 30 minutes and read at 450 nm. The collected values were normalized to blank wells. Then the relative cell viability values were

normalized to the DMSO-treated wells. Graphpad Prism 9 software was used to plot the regression fit curves. Note: Replicate values were observed among wells in which cell viability approached zero following treatment especially due to the raw OD values acquired by the microplate reader are limited to three decimal places.

Cell death assay

For cell death assay, cells were seeded in 12-well plate with appropriate confluences and cultured ferroptosis inducers for indicated time, For DOT1L inhibition, cells were pretreated with SGC0946 for 48 hours. The SYTOX Green Nucleic Acid dye (Invitrogen) was added into plates for 15 min incubation at 37 °C. Sytox Green-positive cells were calculated using an inverted fluorescence microscope (Olympus), and images were captured at least three randomly chosen fields. Living and dead cells were counted (cells stained with green were considered as dead cells), eventually the ratio of dead cells/ living cells + dead cells was calculated. Please note: Because cell-death percentages were derived from finite cell counts, identical values could occasionally occur across independent measurements, particularly at very low or very high levels of cell death.

FACS-based Lipid peroxidation assay

Cells were harvested and washed with PBS, then resuspended with PBS containing 2 μM BODIPY 581/591 C11 dye (D3861, Thermo Fisher Scientific) and incubated at 37 °C for 30 min. Cells were then washed twice with PBS followed by resuspending in 200 μl PBS. Lipid ROS levels were analyzed using a Becton, Dickinson FACS Calibur machine through the FL1 channel. In each sample, 10,000 cells were analyzed. Data were then analyzed using FlowJo software.

Oil red O staining

Frozen sections were prepared from fresh liver tissues and stained with Oil Red O working solution. After washing with the rinsing solution, the sections were rinsed with distilled water. To clearly visualize the cellular structure, the nuclei were counterstained with hematoxylin. Finally, the sections were mounted with an aqueous mounting medium and observed under a light microscope.

Immunohistochemistry staining

Fresh liver tissues were first fixed in 4% paraformaldehyde overnight, followed by two washes with PBS and storage in 70% ethanol at 4°C. Subsequently, the tissues were dehydrated and embedded in paraffin. The embedded tissue blocks were sectioned into 5-μm-thick slices for hematoxylin and eosin (H&E) staining or immunohistochemical (IHC) analysis. To detect the expression of 4-hydroxynonenal (4-HNE) or malondialdehyde (MDA) in liver tissues, immunohistochemistry was performed. Specifically, tissue sections were deparaffinized in xylene and rehydrated through a graded alcohol series. The sections were then incubated in a solution containing 2% Tween-20 for 20 minutes. To quench endogenous peroxidase activity and block nonspecific epitopes, the sections were treated with a stimulating buffer containing 5% bovine serum albumin (BSA) for 15 minutes. The sections were incubated separately with primary antibodies against 4-HNE (dilution 1:300) and MDA (dilution 1:200) overnight at 4°C

in a humidified chamber. After incubation, the sections were treated with a biotin-labeled secondary antibody, followed by incubation with SABC reagent for 30 minutes according to the manufacturer's instructions. Antigen detection was visualized using 3,3'-diaminobenzidine (DAB) and counterstained with DAPI. Finally, IHC images were captured using a multispectral whole-slide scanning microscopy system (TissueGnostics, Austria), and the percentage of positive area was quantified using ImageJ software.

Serum ALT and AST assay

Blood samples were collected from mice and allowed to clot at room temperature for 30 minutes. The samples were centrifuged at 4°C, 4000 rpm for 15 minutes to obtain serum for subsequent analysis. The measurements of ALT and AST were performed according to the instructions provided with the assay kits (Solarbio, BC1555; BC6435). Briefly, a standard curve was generated using the standards included in the kit. An appropriate amount of reaction reagent was added to each test sample based on experimental requirements. The mixtures were then mixed thoroughly and allowed to stand at room temperature for about 10 minutes. The absorbance of each sample was measured at a wavelength of 505 nm using a microplate reader. Serum ALT and AST concentrations were calculated from the standard curves and subsequently normalized for each animal to the mean value of the control group. Please note: Due to the calculated and normalized values were reported at finite numerical precision, distinct raw OD505 measurements could occasionally yield identical reported values after transformation and rounding. Thus, repeated numerical values in the processed dataset do not represent duplicated raw measurements.

Serum TG and tissue TG assay

The triglyceride (TG) content in liver tissue and serum was quantified using an enzymatic colorimetric assay kit. A standard curve was generated using the provided standards. Liver tissue samples were weighed and homogenized. Both tissue homogenates and serum were then incubated with the assay working solution. In the reaction, TG is hydrolyzed by lipoprotein lipase to glycerol and free fatty acids. The glycerol is subsequently converted via a series of enzymatic steps into a colored product, the concentration of which is proportional to the original TG concentration. Absorbance was measured at 550 nm. TG concentrations in the tissue homogenate (expressed as μmol/g protein) and in serum (expressed as μmol/L) were determined by interpolation from the standard curve.

Transcriptome sequencing

Total RNA was isolated from mouse liver or cultured cells. Liver datasets included hepatic IR (sham, IR, and IR plus Lipro-1; n = 5 per group), Dox-associated injury (vehicle and 3 Dox doses; n = 5 per group), and MCDD-associated steatohepatitis (NCD and MCDD; n = 5 per group). IR was used as the primary mechanistic model because ferroptosis-sensitive injury was directly evaluated by Lipro-1 rescue; Dox and MCDD datasets served as complementary injury contexts. Cellular datasets included sgNC, sgDOT1L#1, sgDOT1L#2, DMSO, and SGC0946 groups (n = 3). Libraries were prepared with the NEBNext Ultra II Directional RNA Library Prep Kit and sequenced as 150-bp paired-end reads on an Illumina NovaSeq platform. Reads were quality filtered with fastp, aligned using STAR, quantified with featureCounts, and

analyzed with DESeq2 (|log2FC| >0.5 and *P* value <0.05). Functional enrichment was performed with clusterProfiler.

IP-MS based Proteomic analysis

Protein complexes were immunoprecipitated from HEK293T cells co-transfected with Flag-DOT1L and HA-AMPK using ANTI-FLAG® M2 Affinity Gel beads (A2220, Sigma aldrich). After extensive washing, bound proteins were on-bead digested with trypsin. The resulting peptides were separated by nano-liquid chromatography and analyzed by tandem mass spectrometry on a timsTOF Pro (Bruker) mass spectrometer operating in data-dependent acquisition mode.

Raw MS data were processed using MaxQuant1.6.14 against the Human UniProt database. Protein identification required at least two unique peptides with *FDR* < 1% at both peptide and protein levels. Significant interactors were defined by fold-change > 2 and adjusted *p-value* < 0.05 compared to control IgG samples. Bioinformatic analysis was performed using Perseus for statistical analysis and cluster Profiler for GO and KEGG pathway enrichment.

LC-MS for Lipidomic

Cell or liver samples were extracted by an MTBE-based procedure with class-specific internal standards. Extracts were analyzed on a SCIEX ExionLC system coupled to a QTRAP 6500+ mass spectrometer using a Thermo Accucore C30 column. Lipids were quantified in Skyline from peak-area ratios to corresponding internal standards and normalized to protein amount where applicable. For oxidized phospholipids, mouse liver tissues were collected, and phospholipids were prepared and analyzed following established procedures (J Lipid Res. 2008 May;49(5):1137-46). Phospholipids were analyzed by LC-MS using a Dionex Ultimate 3000 HPLC system coupled with a Q-Exactive Hybrid Quadrupole-Orbitrap mass spectrometer (Thermo Fisher Scientific). Phospholipids were separated using a column (Waters ACQUITY BEH HILIC, 100 × 2.1 mm, 1.7 μm) at a flow rate of 0.25 mL·min-1, and the column temperature was maintained at 40 °C. Gradient solvents A (acetonitrile/water, 95/5, v/v) and B (acetonitrile/water, 50/50, v/v) contained 10 mM ammonium formate. The gradient elution was as follows: 0 min, 0% B; 15 min, 50% B; 15.1 min, 100% B; 18 min, 100% B; 18.1 min, 0% B; 28 min, 0% B. Capillary spray voltage, -3.0 kV; capillary temperature, 320 °C; the S-lens RF level, 60. Analysis was performed in full MS negative mode at resolution setting of 70,000 and data-dependent-MS2 mode at resolution setting of 17,500. For MS, the scan range, m/z 114-1700; the maximum ion injection time, 100 ms. For MS2, the collision energy (CE), 24 eV; the maximum ion injection time, 50 ms. An isolation window of 1.0 Da was set for the MS and MS2 scans. Peaks with a signal-to-noise ratio above 3 were matched to oxidized phospholipids in an in-house database, with m/z values matched within 5 ppm for identification. Lipids were further filtered by retention time and confirmed using MS2 analysis, following Lipid Maps guidelines (https://www.lipidmaps.org). Quantitative analysis relies on calibration curves constructed from known amounts of reference standards and corresponding internal standards, including CL(16:0/18:2/18:2/20:4), PC(18:1/18:1), PE(18:1/18:1), PG(18:1/18:1), PI(18:1/18:1), PS(18:1/18:1), CL(14:0/14:0/14:0/14:0), PC(16:0-d31/18:1), PE(16:0-d31/18:1), PG(16:0-d31/18:1), PI(16:0-d31/18:1), PS(16:0-d31/18:1) (*Nat Chem Biol*. 2021;17(4):465-476; *Methods Mol Biol*. 2023; 2712:81-90).

LC-MS based Metabolite measurement

Intracellular GSH, glutathione peroxidase activity, tetrahydrobiopterin, and oxidized/reduced CoQ10 were measured after pharmacological or genetic inhibition of DOT1L. GSH and biopterin species were identified by their characteristic mass-spectrometric transitions, and CoQ10 redox status was calculated from the reduced and oxidized species. All LC–MS/MS analyses were performed at the Center of Drug Analysis and Test, School of Pharmaceutical Sciences, Shandong University, using a validated targeted metabolomics platform.

Specially, for measurement of oxidized and reduced CoQ10, cells were rapidly harvested, washed with ice-cold PBS, collected by centrifugation, and immediately stored at −80°C until analysis. Cell metabolites were extracted under dim light using ice-cold isopropanol/methanol (1:1, v/v) containing 0.1% butylated hydroxytoluene (BHT) and isotope-labeled internal standards (CoQ10-d_9) to prevent oxidation of ubiquinol-10 (CoQ10H2) and ensure quantitative accuracy. After vigorous mixing and centrifugation at 15,000 × g for 10 min at 4°C, the supernatants were collected, dried under nitrogen, and reconstituted for LC–MS/MS analysis. Chromatographic separation was performed on a reversed-phase C18 column using a UHPLC system with water containing 10 mM ammonium acetate as mobile phase A and methanol/isopropanol (1:1, v/v) as mobile phase B. The gradient program was set as follows: 70% B at 0 min, increased to 85% B at 2 min, 98% B at 8 min, maintained at 98% B until 12 min, and returned to 70% B at 12.5 min. The injection volume of standards and samples was 1 μl. Mass spectrometric detection was performed using a triple quadrupole mass spectrometer equipped with an APCI source operated in positive ion mode. Quantification was performed using multiple reaction monitoring (MRM) transitions of m/z 863.5→197 for ubiquinone-10 and m/z 865.5→197 for ubiquinol-10. Metabolite concentrations were calculated based on calibration curves generated from authentic standards and normalized to internal standards. The CoQ10 redox state was evaluated by calculating the ratio of reduced CoQ10 to total CoQ10 (CoQ10H2/ [CoQ10H2 + CoQ10] × 100%).

For BH4 analysis, cell pellets were extracted with ice-cold 0.1 M trichloroacetic acid containing antioxidant reagents (1 mM dithiothreitol and 1 mM EDTA) under dim light to prevent oxidation of tetrahydrobiopterin. For glutathione measurement, metabolites were extracted using ice-cold 80% methanol containing isotope-labeled internal standards (13C2, 15N GSH). Extracts were vortexed, centrifuged at 15,000 × g for 10 min at 4°C, and the supernatants were collected for LC–MS/MS analysis. Chromatographic separation was performed using a reversed-phase C18 column (2.0 × 150 mm, 5 μm) with a mobile phase consisting of water containing 0.1% formic acid (mobile phase A) and acetonitrile containing 0.1% formic acid (mobile phase B). The gradient elution was programmed as follows: 0–2 min, 2% B; 2–8 min, 2–50% B; 8–10 min, 50–95% B; 10–12 min, 95% B; and 12–15 min, returned to 2% B for column equilibration. Mass spectrometric detection was performed using a triple quadrupole mass spectrometer equipped with an electrospray ionization source operated in positive ion mode. Quantification was performed using multiple reaction monitoring (MRM) transitions for BH4 (m/z 206.1→166) and reduced glutathione (GSH; m/z 304→201). Metabolite concentrations were calculated based on calibration curves generated from authentic standards and normalized to corresponding internal standards or cellular protein content. The BH4 and GSH levels were used as indicators of intracellular redox homeostasis.

Epigenetic small-molecule library screen

For Epigenetic small-molecule library screen, HepG2 cells were seeded in 96-well plates at 10,000 cells per well and cultured for 24 hours. Compounds from the epigenetic library (consist of 250 Epigenetic-related inhibitors) were delivered using a concentration-gradient design, with an initial 10 μL aliquot of 100 μM intermediate concentration added to 90 μL of culture medium, yielding a final concentration of 10 μM. Each plate included DMSO controls in columns 1 and 12. Following 48-hour compound pretreatment, cells were exposed to 5 μM RSL3. Cell viability was monitored hourly by microscopy, with the assay terminated when control group mortality reached approximately 50%. Viability was quantified using CCK-8 assay after 30-minute incubation, and OD450 values were recorded for subsequent IC50 calculation and hit identification.

CRISPR screen and high-throughput sequencing

For comprehensive human transcription factors (TFs) loss-of-function screen, lenti-human-TF-gRNA-puromycin library was received as a gift from Chunliang Li (Addgene #162275; http://n2t.net/addgene:162275; RRID: Addgene162275). This library contains 11,364 sgRNAs for 1,639 human TF genes (each gene with 7 sgRNAs) and 100 non-targeting gRNAs as control. Library amplification, lentiviral packaging, and titration were all done according to the standard protocol. Cas9 overexpression (OE) A375 cell lines were constructed by transfection with lentiCas9-Blast into A375 cells. For transduction, 2 × 10^7 Cas9 OE A375 cells (about 500 × coverage) were infected with the TF library at a multiplicity of infection (MOI) of around 0.3. 48h after transduction, T0 cells were harvested. The rest cells were selected with 1.0 ug/mL puromycin for 72h, and 1 × 10^7 cells were passed every 48–56h for 14 days. Then, 8 × 10^6 cells were treated with DMSO or 200nM, 400nM and 600nM RSL3 for 7 days. After indicated treatment, live cells were collected, and genomic DNA was isolated using the Wizard Genomic DNA Purification Kit (Promega, A1120).

The sgRNA libraries were constructed using a two-step PCR amplification. Genomic DNA samples were amplified with sgRNA-specific primers containing bridge sequences using Q5 High-Fidelity DNA Polymerase (NEB). Primary PCR products were pooled, purified with magnetic beads, and subjected to secondary PCR with index primers. The final libraries (~280 bp) were quality-controlled by agarose gel electrophoresis and Qubit quantification. For sequencing preparation, end repair and adapter ligation were performed on purified PCR products followed by additional amplification with P5/P7 primers. Multiplexed libraries were sequenced on Illumina platforms (HiSeq Xten/Novaseq) with PE150 configuration.

Paired-end reads were merged using FLASH, and sgRNA sequences were extracted using custom scripts based on flanking sequences. Read counts were quantified with MAGeCK, followed by assessment of mapping efficiency, sequencing depth, and coverage. Count normalization and quality control including PCA were performed. Differential gene analysis was conducted using MAGeCK's MLE algorithm (for datasets with baseline controls) or RRA algorithm (for non-baseline datasets) with control sgRNA normalization. Functional enrichment analysis (KEGG/GO) was performed through GSEA, and results were visualized accordingly.

ATAC-Seq Data Processing and Analysis

Hepatic tissues were collected from male C57BL/6J mice subjected to three experimental conditions: sham operation, ischemia-reperfusion (IR) injury, and IR injury with Lipro-1 treatment (n=3 biologically independent samples per group). Nuclei were isolated following established protocols and subjected to tagmentation using the Illumina Tagment DNA TDE1 Enzyme and Buffer Kits according to manufacturer's specifications. The resulting libraries were sequenced on an Illumina platform. For data analysis, raw sequencing reads were processed through Cutadapt (v1.9.1) for adapter trimming and quality control. Quality-filtered reads were aligned to the mm10 reference genome using Bowtie2 (v2.2.6). Peak calling was performed with MACS2, and differential accessibility analysis was conducted using edgeR (v3.4.6). Functional annotation of peaks was carried out through GO and KEGG enrichment analyses with GOSeq (v1.34.1) and custom scripts, respectively. Peak distribution and overlap analyses were performed using HOMER and BEDTools (v2.25.0).

CUT&Tag Library Preparation and Data Analysis

H3K79me2 CUT&Tag was performed in sgNC, sgDOT1L#1, and sgDOT1L#2 cells using 2 biologically independent replicates per group. Cells were immobilized on concanavalin A beads, permeabilized, incubated with anti-H3K79me2 antibody and pA-Tn5, tagmented, and subjected to library amplification. Reads were aligned with Bowtie2, peaks were called with MACS2, and differential enrichment was analyzed with MAnorm2. Genome-browser tracks were displayed on identical scales within each comparison.

Primary hepatocyte isolation

Mouse hepatocytes were isolated using the two-step perfusion technique. In brief, the liver was perfused with 30ml of perfusion buffer (Hank's balanced salt solution (HBSS) (Cat#B430KJ, BasalMedia), EGTA 500 nM) through the portal vein at a flow rate of 15 ml/min, followed by 25 ml of enzyme buffer (Cat#L170KJ, BasalMedia), Collagenase Type IV (Cat#C5138, Sigma, 1 mg/mL), CaCl2, 1 M) at the same flow rate. After perfusion, the liver was removed from the abdominal cavity and hepatocytes were released into the William’s E medium supplemented with 2% penicillin-streptomycin using sterile surgical scissors. Cell suspension was filtered through a 70 μm cell strainer. After centrifugation, hepatocytes were purified at low-speed centrifugation (100×g, 3 min) then the pellets were dissociated into single-cell suspension. Finally, primary hepatocytes were seeded into collagen I-coated well plates. The cells are allowed to attach for 4-6 hours before replacing the medium to remove non-adherent hepatocytes.

Supplementary Tables

Table S1. Antibodies used in this paper.

Antibodies	Source	Catalog#
DOT1L (D1W4Z) Rabbit mAb	Cell Signaling Technology	77087
KMT4/Dot1L Rabbit Recombinant mAb	Selleck	A5617
Histone H3 (D1H2) XP® Rabbit mAb	Cell Signaling Technology	4499
Di-Methyl-Histone H3 (Lys79) (D15E8) XP® Rabbit mAb	Cell Signaling Technology	45139
AMPKα (D5A2) Rabbit mAb	Cell Signaling Technology	5831
Phospho-AMPKα (Thr172) (40H9) Rabbit mAb	Cell Signaling Technology	2535
Phospho-AMPK Substrate Motif [LXRXX (pS/pT) MultiMab® Rabbit mAb mix	Cell Signaling Technology	5759
PAFAH Polyclonal antibody	Proteintech	15526-1-AP
ALDH3B1 Rabbit pAb	Immunoway	YT0190
PLCXD3 Polyclonal Antibody	Invitrogen	PA5-71235
Monoclonal ANTI-FLAG® M2	Sigma Aldrich	F1804
HA-Tag (C29F4) Rabbit mAb	Cell Signaling Technology	3724
NRF2 Polyclonal antibody	Proteintech	16396-1-AP
Anti-Glutathione Peroxidase 4	Abcam	ab125066
xCT/SLC7A11 (D2M7A) Rabbit mAb	Cell Signaling Technology	12691
Rabbit Monoclonal GCLC antibody	Abcam	ab190685
DHODH Polyclonal antibody	Proteintech	14877-1-AP
GCH1 Polyclonal antibody	Proteintech	28501-1-AP
FSP1 Polyclonal antibody	Proteintech	20886-1-AP
MLLT3/AF9 Polyclonal antibody	Proteintech	12825-1-AP
Mono-Methyl-Histone H3 (Lys79)	Cell Signaling Technology	12522
Tri-Methyl-Histone H3 (Lys79)	Cell Signaling Technology	74073
Di-Methyl-Histone H3 Antibody Sampler Kit	Cell Signaling Technology	9847
Tri-Methyl Histone H3 Antibody Sampler Kit	Cell Signaling Technology	9783
Anti Malondialdehyde monoclonal antibody	Jaica	MMD-030n
4-Hydroxynonenal Monoclonal Antibody	Thermo	MA5-27570
HSP90 Monoclonal antibody	Proteintech	60318-1-Ig
Beta Actin Monoclonal antibody	Proteintech	66009-1-Ig
GAPDH Monoclonal antibody	Proteintech	60004-1-Ig

Table S2. Chemical reagents used in this paper.

Chemical reagents	Source	Catalog#
ATP Solution, 100 mM (0.25 mL)	Thermo Scientific™	R0441
AMPK (α1, β1, γ1) Protein, active	Sigma Aldrich	14-840-M
PF-05175157	Selleck	S6672
Fatostatin HBr	Selleck	S8284
Z-VAD-FMK	Selleck	S7023
Doxorubicin (DOX) HCl	Selleck	S1208
Cherry Pick Library	Selleck	L2000
FINO2	Selleck	E1244
RSL3	Selleck	S8155
ML162	Selleck	S4452
ML210	Selleck	S0788
Liproxstatin-1(Lipro-1)	Selleck	S7699
Ferrostatin-1(Fer-1)	Selleck	S7243
EPZ5676	Selleck	S7062
SGC 0946	Selleck	S7079
Metformin	Selleck	S5958
Metformin HCl	Selleck	S1950
A-769662	Selleck	S2697
Ex229 (991)	Selleck	S8654
Compound C	Selleck	S7840
RPMI Medium 1640 basic	Gibco	A4192301
DMEM basic	Gibco	A4192101
Opti-MEM	Gibco	31985070
Fetal Bovine Serum	Sigma Aldrich	F0193
Penicillin-Streptomycin Solution	Viva cell	C3420
Trypsin EDTA Solution A	Viva cell	C3530
Glutamic-pyruvic Transaminase Activity Assay Kit	Solarbio	BC1555
Aspartate Aminotransferase Activity Assay Kit	Solarbio	BC6435
Triglyceride Content Assay Kit	Solarbio	BC0625
KOD -Plus- Mutagenesis Kit	Toyobo	SMK-101

Table S3. Recombinant DNA used in this paper.

Recombinant DNA	Source	Catalog#
pMD2.G	Addgene	12259
psPAX2	Addgene	12260
lentiGuide-Puro	Addgene	52963
lentiCas9-Blast	Addgene	52962
lentiCRISPR v2	Addgene	52961

Table S4. sgRNA oligonucleotides used in this paper.

Oligonucleotides	Forward (5'-3')	Reverse (5'-3')
sgNC	CACCGCCCCGCCGCCCTCC CCTCC	AAACGGAGGGGAGGGCGGC GGGGC
sgDOT1L#1	CACCGGCTGAGACTGAAGT CGCCCG	AAACCGGGCGACTTCAGTCT CAGCC
sgDOT1L#2	CACCGGGGAGACGGCTTCT TCACGG	AAACCCGTGAAGAAGCCGTC TCCCC
sgACACB#1	CACCGTGATGACTACTCCT CCGACG	AAACCGTCGGAGGAGTAGTC ATCAC
sgACACB#2	CACCGTAGGGAGTTTCTCC GCCGAC	AAACGTCGGCGGAGAAACTC CCTAC
sgACACA	GCTGGTGCTATCTATCCAT	GCTGGTGCTGTCTATCCGT
sgPLCXD3#1	CACCGCTTCCTGGGCAAAA ATCGCT	AAACAGCGATTTTTGCCCAG GAAGC
sgPLCXD3#2	CACCGACTTCCTGGGCAAA AATCGC	AAACGCGATTTTTGCCCAGG AAGTC
sgPLCXD3#3	CACCGACGAGCTGAAATTA GCCGAC	AAACGTCGGCTAATTTCAGC TCGTC
sgPLA2G7#1	CACCGTCTGTACAACCAAC GGAATA	AAACTATTCCGTTGGTTGTAC AGAC
sgPLA2G7#2	CACCGAGGCGATCATTATC TTGGGA	AAACTCCCAAGATAATGATC GCCTC
sgALDH3B1#1	CACCGTGCGGGAGGCCTTC CACGCG	AAACCGCGTGGAAGGCCTCC CGCAC
sgALDH3B1#2	CACCGCTCAGACACCTCCG ACTCGA	AAACTCGAGTCGGAGGTGTC TGAGC
sgGPX4	CACCGAGAGATCAAAGAG TTCGCCG	AAACCGGCGAACTCTTTGAT CTCTC
sgSLC7A11#1	CACCGCTTGCATATGTATA TCCAT	AAACATGGATATACATATGC AAGC
sgSLC7A11#2	CACCGCGCACTCACCAAAT AGTGAC	AAACGTCACTATTTGGTGAG TGCGC
sgFSP1#1	CACCGCACTCTCATTCACT CCCAAG	AAACCTTGGGAGTGAATGAG AGTGC
sgFSP1#2	CACCGCCAGCGCTCACGGT TCATCG	AAACCGATGAACCGTGAGCG CTGGC
sgDHODH#1	CACCGGTGACTCCAAAACC TCAGGA	AAACTCCTGAGGTTTTGGAG TCACC
sgDHODH#2	CACCGGAGTCTTGAAATCT GGCCCG	AAACCGGGCCAGATTTCAAG ACTCC
sgGCH1#1	CACCGTCCCCGAGCGGGAT CCGCCG	AAACCGGCGGATCCCGCTCG GGGAC

Continued:

Oligonucleotides	Forward (5'-3')	Reverse (5'-3')
sgGCH1#2	CACCGAACCAAGTGATGC TCACACA	AAACTGTGTGAGCATCACTTG GTTC
sgACSL4	CACCGAAGTGTGTGACAG AGCGATA	AAACTATCGCTCTGTCACACA CTTC
sgNRF2#1	CACCGTATTTGACTTCAGT CAGCGA	AAACTCGCTGACTGAAGTCA AATAC
sgNRF2#2	CACCGCGATGTGACCGGG AATATC	AAACGATATTCCCGGTCACAT CGC
sgPRKAA1	CACCGGCTGTCGCCATCTT TCTCC	AAACGAAGATCGGCCACTAC ATTC
sgPRKAA2	CACCGTAATCCGAAATCG GCTATCT	AAACAGATAGCCGATTTCGG ATTAC
sgAF9#1	CACCGATGGTGTTCGTACG CGGTC	AAACGACCGCGTACGAACAC CATC
sgAF9#2	CACCGACTGGATGGTGTTC GTACG	AAACCGTACGAACACCATCC AGTC
Human Transcription Factor Knockout Library	Addgene	162275

351 **Table S5. Primers used in this paper.**

Primers	Forward (5'-3')	Reverse (5'-3')
qPCR Primers for Human Genes		
hPLA2G7	TCATCAGCATGGGTCAACAAAA	CCAAAGGGTGTCAAGGCGAT
hPLCD4	ACTTCAGAATGACGGCATGAC	CCCTCGCATCCATATCTGGG
hPLD1	GAGCCACGGGTAAATACCTCT	CCGCGTGTCCAGATTTTCTATG
hPLCL1	AAAGTCCGGCCAAATTCTCG	TTTCCGTGTTTTTCCCCAGTC
hPLCL2	TTCAGAACTCAAAAAGGTTCGCT	GCTGCGGAATATGTCTGTGTT
hPLCG1	GGAAGACCTCACGGGACTTTG	GCGTTTTCAGGCGAAATTCCA
hPLCG2	TCCACCACGGTCAATGTAGAT	CCCTGGGCGGATTTCTTTTAT
hPLCXD1	CCCATTTCGCACGAGGAGTC	CGGACCATTTCAGCACGACA
hPLCXD3	CTCAGGACCTACTGGAGAGGC	GAGACCCCGACAATGAACTCT
hPLCE1	GCTTCTTAACACGGGACTTGG	CTTCAAGGGCATTGTGCTCTC
hPLCB2	ATCCGGGATACTCGCTTTGG	ACCTTCCACAACTTCGTCTCC
hPLCH1	TCAAGCTGAAACGTGGAACCA	CTCACTCTTCCTAGAGGGTCG
hPLA2G4C	TGCCGGAGTCTCATTTGTCC	GGGTGAACTCGAACCAGGTC
hDGAT2	ATTGCTGGCTCATCGCTGT	GGGAAAGTAGTCTCGAAAGTAGC
hSCD5	TGCGACGCCAAGGAAGAAAT	CCTCCAGACGATGTTCTGCC
hLPCAT1	CGCCTCACTCGTCCTACTTC	TTCCCCAGATCGGGATGTCTC
hALDH1A1	GCACGCCAGACTTACCTGTC	CCTCCTCAGTTGCAGGATTAAAG
hALDH3B1	GCCCTGGAACTATCCGCTG	CGTTCTTGCTAATCTCCGATGG
hACACA	ATGTCTGGCTTGCACCTAGTA	CCCCAAAGCGAGTAACAAATTCT
hACACB	CAAGCCGATCACCAAGAGTAAA	CCCTGAGTTATCAGAGGCTGG
hHMGCS1	GATGTGGGAATTGTTGCCCTT	ATTGTCTCTGTTCCAACTTCCAG
hSREBF1	ACAGTGACTTCCCTGGCCTAT	GCATGGACGGGTACATCTTCAA
hSREBF2	CCTGGGAGACATCGACGAGAT	TGAATGACCGTTGCACTGAAG
hGAPDH	GGAGCGAGATCCCTCCAAAAT	GGCTGTTGTCATACTTCTCATGG
hACTB	CATGTACGTTGCTATCCAGGC	CTCCTTAATGTCACGCACGAT
qPCR Primers for Mouse Genes		
mPtgs2	TGAGCAACTATTCCAAACCAGC	GCACGTAGTCTTCGATCACTATC
mChac1	CTGTGGATTTTCGGGTACGG	CCCCTATGGAAGGTGTCTCC
mDot1l	CAACTGCAAACATCACTACGGA	TCACCTCGTTCCAGTGTGTAT
mActb	GGCTGTATTCCCCTCCATCG	CCAGTTGGTAACAATGCCATGT
mAf9	CGTCTTCCACTTGCACGAAAG	CCCGGACTCTTCTACCTTGTAA
Primers for ChIP-qPCR		
PLA2G7*	ACAGCCCGCGCGCAGCCCA	GTGGCACCATCTTGGGAGCTGAG
PLA2G7#	GGCATCTCATGGGTTTATAGTTG	AGAATCAGACTGAGAGCTTGG
ALDH3B1*	GGGCCACCAGGCAGAGCGG	TCGAAGGCTGACTTGTGCAGGTCC
ALDH3B1#	AACTGCGACCCCCAGACC	GCAGCCGCTGGAACTGTTTC
PLCXD3*	GCACGATGGCCTCGTCTC	ATTCCAGCTCCTAGCTGGC
PLCXD3#	AGGGATCGTTTTTTATATCTCAG	AAACTCCAAGTAGTGCTATCAAG

Continued:

Primers for DOT1L Site-mutant		
	Forward (5'-3')	Reverse (5'-3')
P271L	TCGAAACTCTTTGCACCTCTGA ACTTCAGA	GGACACGATTCTGCCACCTTCCT TCATGTT
P505L	AAGACCCTCCAGTACAAGGCC AGCCTGCAG	TGTGTATGCCAGGAACTGCAGG TACTGGAT
S786A	CACCTGGCGCAGGACCACACG GTGCC	CCGCCTCAGCACAATCTTGGCC GGGG
M55L	CTCGCTCTGGAGAATTACGTTT TAATTGAC	CTTGAGATCCGGGATTTCTTCAC AGACCCA

*Primers were designed to promoter-proximal regions approximately 2 kb upstream of the transcription start site; # Primers were designed to gene-body regions.

Table S6. Software or websites used in this paper.

ImageJ	National Institutes of Health, NY, USA	https://imagej.net/
SPSS 26.0	IBM, Chicago, IL, USA	https://www.ibm.com/cn-zh
GraphPad Prism 9	GraphPad Software,CA, USA	https://www.graphpad.com/
BioRender	Information Technology Company, Toronto, ON, Canada	https://biorender.com
CRISPOR	Concordet and Haeussler	https://crispor.gi.ucsc.edu/crispor.py
PrimerBank	Harvard University	https://pga.mgh.harvard.edu/primerbank/
Flowjo	BD Biosciences	https://www.flowjo.com/

358 **Table S7. Patient information used in this paper.**

Case	Sex	Age (years)	Diagnosis	Background liver status	Child–Pugh class	Previous hepatic surgery	Surgical procedure	Single-clamping ischemia duration (min)	Total ischemia time (min)	Ischemia method
1	Female	57	Intrahepatic cholangiocarcinoma	No cirrhosis or chronic liver disease	A	None	Radical resection of intrahepatic cholangiocarcinoma	15	30	Intermittent Pringle maneuver
2	Male	46	Intrahepatic cholangiocarcinoma	Mild hepatic steatosis	A	None	Radical resection of intrahepatic cholangiocarcinoma	15	30	Intermittent Pringle maneuver
3	Female	78	Intrahepatic cholangiocarcinoma	No cirrhosis or chronic liver disease	A	None	Radical resection of intrahepatic cholangiocarcinoma	15	25	Intermittent Pringle maneuver
4	Female	50	Intrahepatic bile duct stones	No cirrhosis or chronic liver disease	A	None	Partial hepatectomy	20	20	Intermittent Pringle maneuver
5	Male	47	Intrahepatic bile duct stones	No cirrhosis or chronic liver disease	A	None	Partial hepatectomy	20	20	Intermittent Pringle maneuver
6	Male	41	Intrahepatic bile duct stones	No cirrhosis or chronic liver disease	A	None	Partial hepatectomy	20	20	Intermittent Pringle maneuver
7	Female	49	Intrahepatic bile duct stones	No cirrhosis or chronic liver disease	A	None	Partial hepatectomy	20	20	Intermittent Pringle maneuver
8	Female	56	Intrahepatic bile duct stones	No cirrhosis or chronic liver disease	A	None	Partial hepatectomy	15	20	Intermittent Pringle maneuver
9	Male	55	Intrahepatic bile duct stones	No cirrhosis or chronic liver disease	A	None	Partial hepatectomy	20	20	Intermittent Pringle maneuver
10	Female	43	Intrahepatic bile duct stones	No cirrhosis or chronic liver disease	A	None	Partial hepatectomy	20	20	Intermittent Pringle maneuver

Case	Sex	Age (years)	Diagnosis	Background liver status	Child–Pugh class	Previous hepatic surgery	Surgical procedure	Single-clamping ischemia duration (min)	Total ischemia time (min)	Ischemia method
11	Male	67	Hepatocellular carcinoma	HBV-related cirrhosis	A	Previous antiviral therapy	Hepatocellular carcinoma resection	10	20	Intermittent Pringle maneuver

359

Supplementary Figure legends

Suppl. Fig. S1. Chromatin-accessibility remodeling across liver injury models, related to Figure 1. (A) Schematic illustration of epigenetic regulation of chromatin accessibility and transcriptional activity. **(B)** Principal component analysis of ATAC-seq profiles from control, hepatic ischemia–reperfusion (IR), and IR plus Lipro-1 groups. **(C)** Heatmap showing differential promoter accessibility patterns among control, IR, and IR+Lipro-1 groups with corresponding signal intensity profiles. **(D)** Representative normalized ATAC-seq tracks at the *Slc25a48*, *Fads2*, *Scd1*, *Apoa5*, *Nfe2l2*, and *Gch1* loci; shaded regions indicate differential promoter-proximal accessibility. **(E)** GO enrichment analysis of genes associated with IR-induced differential chromatin accessibility, highlighting ferroptosis- and lipid metabolism-related pathways. ATAC-seq included 3 biologically independent mice per group. Differential expression, accessibility, and pathway enrichment were analyzed using DESeq2, edgeR, and clusterProfiler, respectively, with Benjamini–Hochberg correction.

Suppl. Fig. S2. Transcriptomic changes across Dox- and MCDD- induced liver injury models, related to Figure 1. (A, B) Heatmaps showing differentially expressed genes (DEGs, log2FC >0.5 or <-0.5 and P value <0.05) between doxorubicin (Dox) versus DMSO groups (A) and MCDD versus NCD groups (B). **(C, D)** Pathway enrichment analysis of differentially expressed genes in Dox versus DMSO (C) groups and MCDD versus NCD livers (D). N = 5 mice per group in A and B.

Suppl. Fig. S3. H3K79 methylation is increased in multiple liver injury models, related to Figure 1. (A–C) Representative immunoblots and densitometric quantification of the indicated histone methylation marks in liver tissues from sham-, hepatic ischemia–reperfusion (IR)-, and IR plus Lipro-1–treated mice (A); vehicle- and doxorubicin-treated mice (B); and normal chow diet (NCD)- and methionine–choline-deficient diet (MCDD)-fed mice (C). Histone methylation signals were normalized to total histone H3 and expressed relative to the IR group in A and the corresponding control group in B and C. IR increased H3K79me2, which was reduced by Lipro-1, whereas doxorubicin and MCDD increased H3K79me2 and H3K79me3. Each dot represents an individual mouse; n = 3 mice per group in A and n = 4 mice per group in B and C. Data are presented as mean ± SD. Statistical significance in A was determined by two-way ANOVA followed by Dunnett's multiple-comparisons test, with comparisons performed against the IR group within each histone methylation mark. Two-tailed unpaired Student's t test was used in B and C. † indicates the control value normalized to 1. * $P < 0.05$, ** $P < 0.01$, *** $P < 0.001$; ns, not significant.

Suppl. Fig. S4. DOT1L promotes ferroptotic susceptibility through its H3K79 methyltransferase activity, related to Figure 2. (A and B) Workflow and MAGeCK β-score analysis of a pooled CRISPR screen performed in Cas9-expressing A375 cells at approximately 500-fold library coverage following treatment with 200, 400, or 600nM RSL3 for 7 days continuously; DOT1L was enriched among resistance-associated hits. **(C and D)** Immunoblot analysis of H3K79me2 in SNU449 cells or primary mouse hepatocytes (C) and A375 or HT1080 cells (D) treated with DMSO, SGC0946(10μM), or EPZ5676(10μM) for 24h. **(E–L)** Cell viability

or SYTOX Green–based cell-death analysis in HepG2, SNU449, THLE-2 and AML12 cells exposed to RSL3(2μM for cell death), ML162(2μM for cell death), or Erastin(2.5μM for cell death) with or without DOT1L inhibition(10μM, pretreated for 24h) and Lipro-1(2μM) for 6-12h. **(M)** Lipid peroxidation analysis in sgNC and sgDOT1L HepG2 cells treated with RSL3(500 nM) and Lipro-1(2μM) for 4h. **(N and O)** Cell viability analysis in A375 or HT1080 cells exposed to RSL3(0-10μM) or ML162(0-10μM) with or without DOT1L inhibition(10μM, pretreated for 24h) for 6h. Immunoblots are representative of 3 independent experiments. Quantitative data are mean ± SD from 3 biologically independent experiments in E–H and J-M. Dose-response curves were fitted by 4-parameter nonlinear regression. For comparisons under RSL3 treatment, statistical significance was determined by one-way ANOVA followed by Dunnett's multiple-comparisons test in E–H and J-M. Exact P values are shown; ns, not significant.

Suppl. Fig. S5. DOT1L promotes ferroptotic susceptibility through its H3K79 methyltransferase activity, related to Figure 2.
(A) Cell viability analysis in A375 or HT1080 cells exposed to Erastin(2.5μM) with or without DOT1L inhibition (10μM, pretreated for 24h) for 6h. **(B–E)** Validation of DOT1L depletion and dose-response analysis of RSL3-, ML162-, and erastin-induced cytotoxicity in HT1080 and A375 cells expressing sgNC or 2 independent DOT1L-targeting sgRNAs (treatment with ferroptosis inducers for 6h). **(F–H)** SYTOX Green–based cell-death assays and C11-BODIPY 581/591–based lipid-peroxidation measurements following RSL3(2μM for cell death, 500nM for C11) treatment with or without Lipro-1(2μM) for 3h (C11-BODIPY assay) or 6h (cell death assay). **(I)** Immunoblot analysis of H3K79me2 restoration in DOT1L-knockout HepG2 cells re-expressing wild-type or catalytic mutant DOT1L variants. **(J)** Cell viability and ferroptotic cell death analysis in DOT1L-rescued HepG2 cells treated with RSL3(2μM for cell death) with or without Lipro-1(2μM) for 6h. **(K and L)** Immunoblot validation and RSL3-response analysis (1μM for 6h) of DOT1L-knockout A375 cells re-expressing wild-type or catalytic mutant DOT1L variants. **(M)** Schematic model illustrating DOT1L catalytic activity-dependent regulation of ferroptosis sensitivity through H3K79 methylation and lipid metabolic remodeling. Immunoblots are representative of 3 independent experiments. Quantitative data are mean ± SD from 3 biologically independent experiments in C–H and J and 4 biologically independent experiments in L. Dose-response curves were fitted by 4-parameter nonlinear regression; For comparisons under RSL3 treatment, statistical significance was determined by one-way ANOVA followed by Dunnett's multiple-comparisons test in C–H, J and L, with sgNC as the reference group. Exact P values are shown; ns, not significant.

Suppl. Fig. S6. DOT1L inhibition or depletion protects against doxorubicin- and MCDD-induced liver injury, related to Figure 3. (A) Immunoblot analysis of hepatic H3K79me2 levels following indicated treatments. **(B–E)** Experimental design (B), representative liver histology and ferroptosis-associated staining (C), serum ALT and AST levels (D), and hepatic *Ptgs2* and *Chac1* mRNA expression (E) in C57BL/6J mice treated with Dox (20 mg/kg for 4 days), Dox plus SGC0946 (SGC0946, 5 mg/kg for 24h), or Dox plus Fer-1 (Fer-1, 10 mg/kg for 1h). **(F)** Western blot analysis of Dot1l protein expression in indicated tissues from C57BL/6 mice 4 weeks after tail vein injection of AAV8-*shCtrl* or AAV8-*shDot1l*. Dot1l expression was examined in brain, lung, liver, kidney, and heart tissues. Hsp90 was used as the loading control. **(G)** Representative immunofluorescence images showing the cellular localization of Dot1l in mouse liver tissues. Liver

sections were co-stained with antibodies against Dot1l and albumin, a hepatocyte marker. Scale bars: 10μm. **(H)** Multiplex immunofluorescence analysis of mouse liver tissues following AAV8-shCtrl or AAV8-shDot1l administration. Liver sections were stained with Dot1l together with cell-type-specific markers, including CD68 (macrophages), CK7 (cholangiocytes), α-SMA (hepatic stellate cells), and CD31 (endothelial cells). Scale bars: 100μm. **(I-K)** Experimental scheme(I), representative H&E, Oil Red O, MDA, and 4-HNE staining (J), and serum ALT/AST quantification (K) in mice receiving hepatocyte-targeted Dot1l knockdown (AAV8-Tbg-*shDot1l*) followed by Dox administration (20 mg/kg for 4 days). **(L-N)** Experimental design and metabolic phenotyping of MCDD-induced steatohepatitis model with or without DOT1L inhibition, including liver/body weight ratio, hepatic triglyceride content, serum ALT and AST levels. Data are presented as mean ± SD (E) or box-and-whisker plots showing median, interquartile range, and minimum-to-maximum values (D, H, I–N). Each dot represents an individual mouse (n = 4–6 mice/group, as indicated). Statistical analyses were performed using ordinary one-way ANOVA followed by Dunnett's multiple-comparisons test in D and E and two-way ANOVA by Šídák's multiple-comparisons test in K and N. Exact P values are shown in the panels. Scale bars: 50 μm.

Suppl. Fig. S7. DOT1L inhibition or depletion protects against doxorubicin- and MCDD-induced liver injury, related to Figure 3. (A) Experimental design of MCDD-induced steatohepatitis model with or without hepatocyte-targeted Dot1l depletion. **(B and C)** Representative H&E, Oil Red O, MDA, and 4-HNE staining (B) and serum ALT/AST levels (C) in MCDD-fed mice treated with AAV8-Tbg-shDot1l (n = 4–6 mice/group, as indicated). **(D and E)** Effects of DOT1L inhibition on diet-induced MASH. Representative H&E, Oil Red O, and MDA staining (D), hepatic triglyceride content, body weight, and serum ALT and AST levels (E) in mice fed NCD or HFD and treated with SGC0946 (5 mg/kg for 24h, n = 5/group). **(F)** Experimental design of AAV8-TBG–mediated Dot1l knockdown in NCD- and HFD-fed mice. **(G and H)** Representative liver staining (G) and quantification of serum ALT, AST, hepatic triglycerides, and body weight (H) in AAV8-shDot1l mice fed NCD or HFD (n = 5/group). **(I)** Schematic representation of perioperative serum collection and paired intraoperative liver tissue sampling from patients undergoing partial hepatectomy. Liver tissues were collected before ischemia and after ischemia/reperfusion. **(J)** Serum ALT and AST levels at indicated perioperative time points (n = 11). **(K)** Immunoblot analysis and quantification of H3K79me2 levels in paired human liver tissues. Statistical analyses were performed using two-way ANOVA by Šídák's multiple-comparisons test in C, E and H. Serum ALT and AST levels were analyzed by one-way repeated-measures ANOVA followed by Dunnett's multiple-comparisons test in J, with T0 as the reference time point. Two-tailed unpaired Student's t test for two-group comparisons (K). Exact P values are shown in the panels. Scale bars: 50 μm.

Suppl. Fig. S8. DOT1L inhibition retains anti-ferroptotic activity after disruption of major canonical ferroptosis-defense pathways, related to Figure 4. (A) Heatmaps showing expression changes of ferroptosis-associated genes in sgDOT1L versus sgNC cells across HepG2, SK-hep1, and A375 cell lines or in cells treated with SGC0946(10μM) versus DMSO for 24h. **(B)** Immunoblot analysis of canonical ferroptosis regulators in HepG2, SK-Hep1, and A375 cells following genetic depletion or pharmacological inhibition of DOT1L (10μM for 24h). **(C–E)** Validation of GCLC depletion (C) and quantification of RSL3-induced lipid peroxidation (500nM

for 3h) (D) and cell death (2μM for 6h) (E) in A375 and HT1080 cells treated with DMSO or SGC0946(10μM, pre-treatment for 24h), with or without Lipro-1(2μM). **(F and G)** FSP1 depletion (F), RSL3-induced cell death (2μM for 6h), and C11-BODIPY 581/591–based lipid-peroxidation (500nM for 3h) analysis (G) in HT1080 cells. **(H–J)** Validation of SLC7A11 knockout (H) and lipid-peroxidation (500nM for 3h) (I) and cell-death (2μM for 6h) (J) analyses following β-mercaptoethanol (β-ME) withdrawal, with or without SGC0946 (10μM, pre-treatment for 24h). **(K–M)** NRF2 depletion (K), RSL3-induced cell death (2μM for 8h) (L), and RSL3 dose-response curves (M) in H1299 cells. Immunoblots are representative of 3 independent experiments. Quantitative data are mean ± SD from 3 biologically independent experiments. For comparisons under RSL3 treatment, statistical significance was determined by one-way ANOVA followed by Dunnett's multiple-comparisons test in C–H, J and L, with sgNC as the reference group. Dose-response curves were fitted using 4-parameter nonlinear regression. Exact P values are shown; ns, not significant.

Suppl. Fig. S9. DOT1L inhibition does not alter major canonical antioxidant-defense systems, related to Figure 4. (A–C) DHODH depletion (A), cell-death analysis (2μM for 6h) (B), and RSL3 dose-response curves (0-10μM for 6h) (C) in A375 cells. **(D-F)** GCH1 depletion (D), RSL3-induced cell death (2μM for 6h) (E) and quantification of RSL3-induced lipid peroxidation (250nM for 3h) (F) in HT1080 cells. **(G-I)** Immunoblot validation of GPX4 knockout (G) and cell viability (H) and quantification of RSL3-induced lipid peroxidation (250nM for 3h) (I) after Ferrostatin-1 (2μM) withdrawal, with or without SGC0946(10μM, pre-treatment for 24h). **(J and K)** Relative intracellular glutathione (GSH) concentrations in HepG2 and SNU449 cells following pharmacological inhibition of DOT1L with SGC0946 (10μM, pre-treatment for 24h) (H) or genetic depletion using 2 independent sgRNAs (I). **(L)** Glutathione peroxidase activity in HepG2 cells after pharmacological (10μM, pre-treatment for 24h) or genetic inhibition of DOT1L. **(M** and **N)** Relative intracellular tetrahydrobiopterin (BH4) (M) and reduced CoQ10 (CoQ10H2) (N) concentrations in SGC0946-treated HepG2 cells (10μM, pre-treatment for 24h) or sgDOT1L HepG2 cells. Each symbol represents an independent biological replicate; n = 3 per group in B, E, F, I and K, n = 4 per group in H, L, M and N, and n = 6 for HepG2 or n = 5 for SNU449 in J. Bar graphs are presented as mean ± SD; box-and-whisker plots in J show the median, interquartile range, and minimum-to-maximum values. For comparisons under RSL3 treatment, statistical significance was determined by one-way ANOVA followed by Dunnett's multiple-comparisons test in B, E–I, with sgNC or DMSO as the reference group. For J-N, two-group comparison were determined by Two-tailed unpaired Student's t test and three group comparisons by one-way ANOVA followed by Dunnett's multiple-comparisons test (with sgNC as the reference group). Exact P values are shown.

Suppl. Fig. S10. DOT1L regulates ferroptosis sensitivity through phospholipid metabolic remodeling, related to Figure 4. (A) Differential lipid abundance analysis in HepG2 cells expressing sgNC or sgDOT1L. **(B)** Volcano plots showing differential lipid species identified by lipidomic analysis in THLE-2 cells treated with SGC0946 (10μM) or DMSO for 24h. **(C)** KEGG pathway enrichment analysis of altered lipid species identified in SGC0946-treated HepG2 cells (10μM, pre-treatment for 24h) or sgDOT1L HepG2 cells. Lipidomic analyses were performed using four biologically independent samples per group for cellular experiments(B). Statistical analyses for lipidomic differential abundance were performed using appropriate multiple-testing correction methods as described in Methods. Enrichment analyses were based on significantly altered lipid

species.

Suppl. Fig. S11. DOT1L-dependent H3K79 methylation restrains phospholipid-remodeling genes independent of ACC signaling, related to Figure 5. (A) qRT-PCR validation of selected lipid-metabolic transcripts in HepG2 vector-control (V2) and DOT1L-knockout cells. Expression was normalized to ACTB and presented as $\log_2$ fold change. **(B–D)** Assessment of ACC signaling: immunoblot validation of ACC double knockout and DOT1L inhibition in SK-Hep1 cells (B) and p-ACC^{S79} and total ACC in HepG2 and SNU449 cells expressing sgNC or two independent DOT1L-targeting sgRNAs (C); RSL3-induced cell death (2μM for 6h) after treatment with the ACC inhibitor PF05175157 (10μM), SGC0946 (10μM), or both, with or without Lipro-1(2μM) for 24h (D). **(E and F)** Representative normalized H3K79me2 CUT&Tag tracks after DOT1L depletion (E) and ATAC-seq tracks after SGC0946 treatment (10μM, pre-treatment for 24h) (F) at the ALDH3B1, PLA2G7, and PLCXD3 loci. DOT1L depletion reduced H3K79me2 enrichment, whereas SGC0946 increased promoter-proximal accessibility. **(G and H)** H3K79me1(G) and H3K79me2(H) ChIP-qPCR at regions approximately 2 kb upstream of the respective transcription start sites; enrichment is expressed as fraction of input, with IgG as the negative control. **(I and J)** H3K79me1 (I) and H3K79me2 (J) ChIP-qPCR at gene-body regions showing maximal differential ChIP-seq enrichment within the PLA2G7, ALDH3B1, and PLCXD3 loci in sgNC and sgDOT1L cells. Immunoblots are representative of three independent experiments. The number of biological replicates in A is indicated by individual points; n = 3 in D, n = 2 biological replicates/group for CUT&Tag and ATAC-seq in E and F, and n = 3 biological replicates in G–J. Bars in G–J show mean ± SD. For comparisons under RSL3 treatment, statistical significance was determined by one-way ANOVA followed by Dunnett's multiple-comparisons test in D. Pairwise comparisons in A used 2-tailed unpaired Student's t tests; G–J used one-way ANOVA followed by Dunnett's multiple-comparison test versus sgNC. Exact P values are shown.

Suppl. Fig. S12. PLA2G7, ALDH3B1, and PLCXD3 mediate DOT1L-dependent phospholipid remodeling and ferroptosis resistance, related to Figure 5. (A–C) Immunoblot validation of target-gene induction after DOT1L depletion in SNU449 cells (A) and qRT-PCR analysis after SGC0946 treatment (10μM, pre-treatment for 24h) in THLE-2 cells (B) or DOT1L overexpression in SNU449 cells (C). **(D–N)** Validation and functional characterization of pooled PLA2G7 (D-H) and ALDH3B1 (I–N) deficient cells by immunoblotting, RSL3 dose-response (0-10μM for 6h), SYTOX Green cell-death (2μM for 6h), and C11-BODIPY 581/591 lipid-peroxidation assays (500nM for 3h), with or without Lipro-1 (2μM). The sgALDH3B1 and sgPLA2G7 cell lines were generated and analyzed in parallel; the corresponding data are presented separately in the figure panels (E, F, L and M) but consolidated in the source data files (E and F) to avoid redundancy. Immunoblots are representative of 3 independent experiments (A, D and J). Quantitative data are mean ± SD from 3 biologically independent experiments; Multiple two-tailed unpaired t tests were used in B and C. For comparisons under RSL3 treatment, statistical significance was determined by one-way ANOVA followed by Dunnett's multiple-comparisons test in E, F and L-N. Dose-response curves were fitted using 4-parameter nonlinear regression. Statistical analyses for lipidomic differential abundance (G and I) were performed using appropriate multiple-testing correction methods as described in Methods. Exact P values are shown.

Suppl. Fig. S13. PLA2G7, ALDH3B1, and PLCXD3 mediate DOT1L-dependent phospholipid remodeling and ferroptosis resistance, related to Figure 5. (A-G) Validation and functional characterization of pooled PLCXD3 deficient cells by immunoblotting, RSL3 dose-response (0-10μM for 6h), SYTOX Green cell-death (2μM RSL3 for 6h), lipidomic and C11-BODIPY 581/591 lipid-peroxidation assays (500nM for 3h), with or without Lipro-1(2μM). **(H)** Cell-death assays (2μM RSL3 for 6h) (upper) and immunoblot validation (down) following re-expression of the corresponding wild-type gene in knockout HepG2 cells. **(I and J)** Immunoblot validation (I) and cell-viability analysis (0-10μM for 6h) (J) of DOT1L-knockout SNU449 cells with combined depletion of PLA2G7, ALDH3B1, and PLCXD3. Immunoblots are representative of 3 independent experiments (B, H and I). Quantitative data are mean ± SD from 3 biologically independent experiments; Statistical analyses for lipidomic differential abundance (A) were performed using appropriate multiple-testing correction methods as described in Methods. Dose-response curves were fitted using 4-parameter nonlinear regression. For comparisons under RSL3 treatment, statistical significance was determined by one-way ANOVA followed by Dunnett's multiple-comparisons test in D-J. Exact P values are shown.

Suppl. Fig. S14. AMPK regulates DOT1L activity and ferroptotic susceptibility through Ser786 phosphorylation and AF9, related to Figure 6. (A) Reciprocal endogenous coimmunoprecipitation of DOT1L and AMPK in SK-Hep1 cells. **(B)** Western blot analysis of DOT1L, p-AMPK, total AMPK, and GAPDH protein levels in HepG2 cells at indicated time points (0–10h) following 991 treatments (10μM). **(C and D)** Exogenous (C) and endogenous (D) immunoprecipitation assays demonstrating AMPK-dependent phosphorylation of DOT1L. **(E–H)** Effects of AMPK activation by 991 (10μM for 1h) or glucose deprivation, and AMPK knockout, on DOT1L abundance and H3K79me2 in the indicated cells. **(I)** Phosphoproteomic analysis comparing AMPKα-knockdown and control cells, highlighting reduced DOT1L Ser786 phosphorylation. **(J and K)** H3K79me2 immunoblotting (10μM A769662 for 16h) and cell-viability heatmap in DOT1L-knockout HepG2 cells reconstituted with vector, $DOT1L^{WT}$, or $DOT1L^{S786A}$ under the indicated pharmacological treatments (2μM RSL3 for 6h). **(L–O)** validation of $DOT1L^{WT}$ and $DOT1L^{S786A}$ re-expression in DOT1L-knockout HT1080 cells (L); RSL3-induced cell death (2μM RSL3 for 6h) and dose-response analysis (0-10μM RSL3 for 6h) (M, N); and *PLA2G7*, *ALDH3B1*, and *PLCXD3* mRNA expression (O). Quantitative data are mean ± SD from 3 biologically independent experiments; For comparisons under RSL3 treatment, statistical significance was determined by one-way ANOVA followed by Dunnett's multiple-comparisons test in M. Dose-response curves were fitted using 4-parameter nonlinear regression. Statistical significance was determined by one-way ANOVA followed by Dunnett's multiple-comparisons test in O. Exact P values are shown.

Suppl. Fig. S15. AMPK regulates DOT1L activity and ferroptotic susceptibility through Ser786 phosphorylation and AF9, related to Figure 6. (A) Schematic representation of human DOT1L domains and functional regions. **(B and C)** Immunoblot analysis of DOT1L subcellular localization following AMPK activation (10μM 991 for 1h) or inhibition (10μM Compound C for 16h) in HepG2 and SNU449 cells. **(D and E)** Co-immunoprecipitation assays evaluating the interaction between DOT1L and AF9 following AMPK activation (10μM 991 for 1h) (D) and with DOT1L S786 mutants (E). **(F–H)** AF9 depletion, RSL3 dose-response analyses (0-10μM for 6h),

and expression of DOT1L-regulated target proteins in SNU449 and HepG2 cells. **(I)** Coimmunoprecipitation of DOT1L and AF10 following 991 treatments (10μM for 1h). **(J)** Working model illustrating AMPK-mediated inhibition of DOT1L activity through Ser786 phosphorylation and subsequent regulation of ferroptosis-associated genes, including *PLA2G7*, *ALDH3B1*, and *PLCXD3*. Immunoblots are representative of 3 independent experiments. Quantitative data are mean ± SD from 3 biologically independent experiments (G); dose-response curves were fitted using 4-parameter nonlinear regression.

Suppl. Fig. S16. AMPK activation suppresses ferroptosis-associated liver injury through a pathway distinct from canonical ACC signaling, related to Figure 7. (A) Immunoblot analysis of ACC, AMPK activation, and H3K79me2 levels in sgNC and ACC double-knockout (ACC DKO) HepG2 and SK-Hep1 cells treated with DMSO or A769662 (10μM for 16h). **(B)** Cell viability analysis of sgNC and ACC DKO HepG2 cells treated with A769662 (10μM pre-treatment for 16h) followed by RSL3(0-10μM for 6h) exposure with or without Lipro-1(2μM). **(C)** Schematic illustration of the experimental design for hepatic ischemia/reperfusion (IR) injury with pharmacological modulation of AMPK and DOT1L activity. Mice were treated with A769662 (10mg/kg), PF05175157 (50mg/kg), and SGC0946 (5mg/kg) respectively at 24h, 16h or 16h prior to IR injury. **(D)** Serum ALT and AST levels in mice subjected to IR injury with indicated treatments (n = 5 mice per group). **(E)** Representative images of H&E staining and MDA immunohistochemical staining of liver tissues from mice subjected to IR injury with indicated treatments. Scale bar: 50 μm. **(F–I)** Experimental scheme (F), representative H&E, Oil Red O, MDA, and 4-HNE staining (G), hepatic triglyceride content (H), and serum ALT/AST levels (I) in NCD- or MCDD-fed mice treated with A769662 (10mg/kg), the ACC inhibitor PF05175157 (50mg/kg), the DOT1L inhibitor SGC0946 (5mg/kg), or the indicated combinations. Immunoblots are representative of 3 independent experiments. Quantitative data are mean ± SD for in vitro assays (n = 3 biologically independent experiments); animal data are box-and-whisker plots showing median, interquartile range, and minimum-to-maximum values (n = 5 mice/group in D and n = 4-8 mice/group in H and I). Dose-response curves were fitted by 4-parameter nonlinear regression; Statistical significance was assessed using one-way ANOVA followed by Šídák's multiple-comparisons test in D, H and I. Exact P values are shown. Scale bars: 50 μm.

Suppl. Fig. S17. AMPK activation suppresses ferroptosis-associated liver injury through a pathway distinct from canonical ACC signaling, related to Figure 7. (A–C) Experimental scheme (A), representative histological staining (B), and serum ALT/AST levels (C) in doxorubicin-treated (20 mg/kg for 4days) mice receiving the indicated single or combined treatments. **(D-F)** Dose-dependent effects of metformin on p-AMPK^{T172} and H3K79me2 (D) and RSL3-induced cell viability (0-10μM for 6h) and death (2.5μM for 6h) in HepG2 cells pretreated with metformin, with or without Lipro-1 (2μM) (E and F). **(G)** Schematic illustration of the experimental design for hepatic IR injury treated with SGC0946 (5mg/kg for 24h), metformin (200mg/kg, 48h, 24h and 1h before ischemia), or their combination. **(H)** Relative mRNA expression levels of ferroptosis-associated genes *Ptgs2* and *Chac1* measured by qRT-PCR (n = 4 mice per group). **(I)** Immunoblot analysis of AMPK activation and H3K79me2 levels in HepG2 cells treated with increasing concentrations of metformin (0-200μM for 24h). **(J–L)** Experimental scheme (J), serum ALT and AST levels (K), and representative H&E, Oil Red O, MDA, and 4-HNE staining (L) in doxorubicin-

treated (20 mg/kg for 4days) mice receiving SGC0946 (5mg/kg, 24h before ischemia), metformin (200mg/kg, 48h, 24h and 1h before ischemia), or both. Immunoblots are representative of 3 independent experiments. Quantitative data are mean ± SD for in vitro assays (n = 3 biologically independent experiments); animal data are box-and-whisker plots showing median, interquartile range, and minimum-to-maximum values (n = 4–7 mice/group in C and n = 5 mice/group in K). Dose-response curves were fitted by 4-parameter nonlinear regression; Statistical significance was assessed using one-way ANOVA followed by Šídák's multiple-comparisons test in C, H and K. For comparisons under RSL3 treatment, statistical significance was determined by one-way ANOVA followed by Dunnett's multiple-comparisons test in F. Exact P values are shown. Scale bars, 50 μm.

Suppl. Fig. S18. DOT1L Ser786 phosphorylation and AF9 regulate AMPK-dependent protection against hepatic ischemia–reperfusion injury, related to Figure 7. (A) Experimental scheme for hepatic DOT1L depletion followed by IR and treatment with DMSO, Lipro-1 (10mg/kg for 1h), or metformin (200mg/kg, 48h, 24h and 1h before ischemia). **(B)** Validation of hepatic *Dot1l* knockdown efficiency by qRT-PCR. **(C and D)** Representative H&E and MDA staining (C) and serum ALT/AST levels (D) in AAV8-Tbg-*shCtrl* and AAV8-Tbg-*shDOT1L* mice subjected to the indicated treatments. **(E)** Experimental scheme for evaluating $DOT1L^{WT}$ and $DOT1L^{S786A}$ in hepatic ischemia–reperfusion injury with or without metformin. **(F and G)** Representative H&E and MDA staining (F) and serum ALT/AST levels (G) in mice expressing Tbg-*control*, Tbg-$Dot1l^{WT}$, or Tbg-$Dot1l^{S786A}$ and subjected to hepatic ischemia–reperfusion (IR) with the indicated PBS, metformin (200mg/kg, 48h, 24h and 1h before ischemia), or Lipro-1 (10mg/kg for 1h) treatments. **(H-J)** Validation of hepatic $DOT1L^{WT}$ and $DOT1L^{S786A}$ expression by immunoblotting and qRT-PCR (H) and DOT1L immunoprecipitation analysis following metformin treatment (200mg/kg, 48h, 24h and 1h before ischemia) (J). Immunoprecipitants were analyzed for the AMPK substrate motif LXRXX (pS/pT), DOT1L, and AF9; input lysates were analyzed for p-$AMPK^{T172}$, H3K79me2, and the indicated controls. Immunoblots are representative of 3 mice per group. Quantitative data include n = 4 mice per group in B and H and n = 5 mice per group in D and G. Box-and-whisker plots show the median, interquartile range, and minimum-to-maximum values. Statistical significance was assessed using one-way ANOVA followed by Šídák's multiple-comparisons test in D and G and two-tailed unpaired Student's t test in B and one-way ANOVA followed by Šídák's multiple-comparisons test in H. Exact P values are shown.

Suppl. Fig. S19. DOT1L Ser786 phosphorylation and AF9 regulate AMPK-dependent protection against hepatic ischemia–reperfusion injury, related to Figure 7.
(A) Experimental scheme for hepatic *Af9* depletion followed by IR and treatment with vehicle, Lipro-1 (10mg/kg for 1h), or SGC0946 (5mg/kg for 24h). **(B and C)** Validation of hepatic *Af9* knockdown efficiency by qRT-PCR (B) and immunoblotting (C). **(D and E)** Representative H&E and MDA staining (D) and serum ALT and AST levels (E) in AAV8-Tbg-*shCtrl* and AAV8-Tbg-*shAf9* mice subjected to the indicated treatments. Immunoblots are representative of 3 mice per group. Quantitative data include n = 6 mice per group in E. Box-and-whisker plots show the median, interquartile range, and minimum-to-maximum values. Statistical analyses were performed using 2-tailed unpaired Student's t test in B and two-way ANOVA by Šídák's multiple-comparisons test in E. Exact P values are shown.

Figure S1.

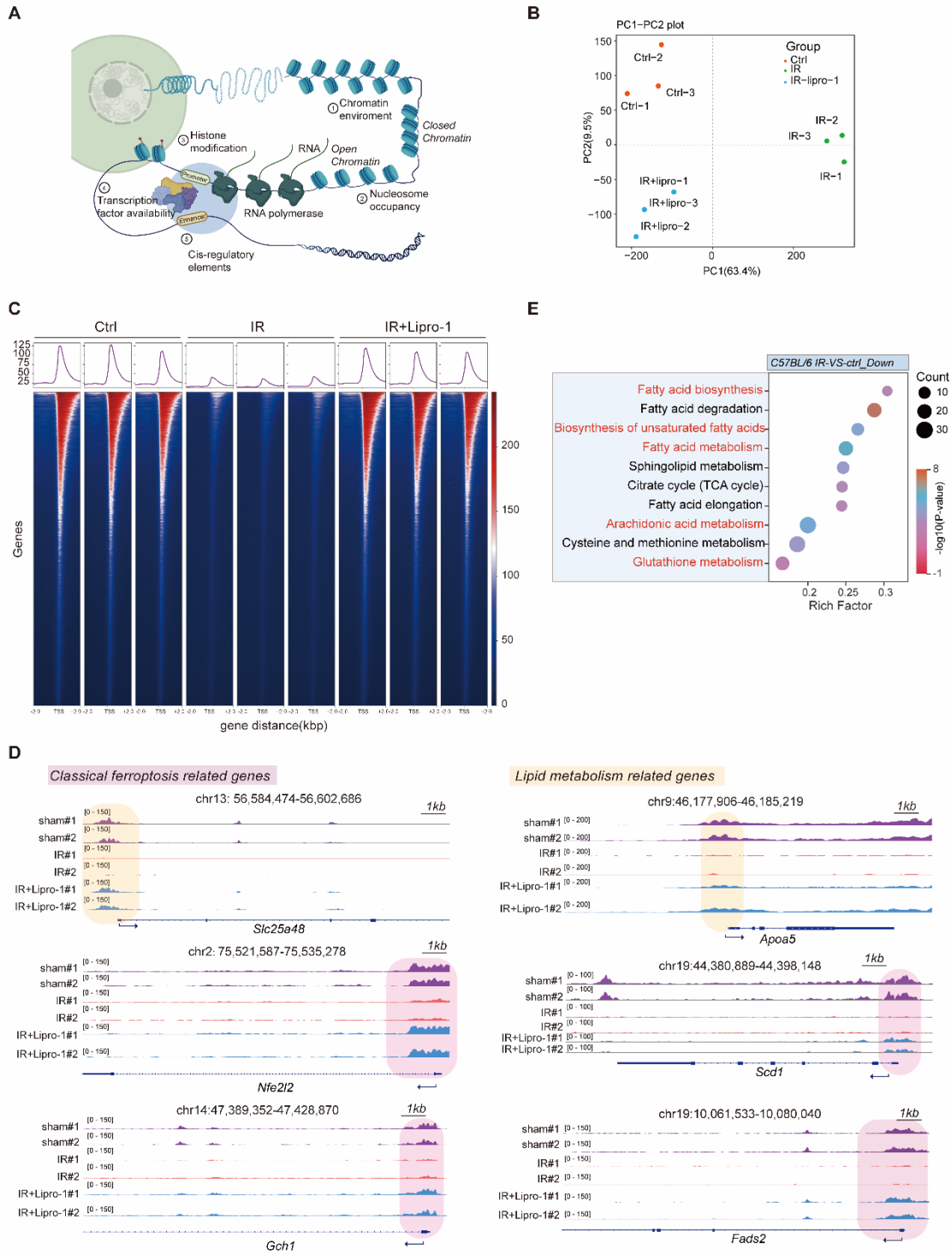

A
Chromatin enviroment
Closed Chromatin
Histone modification
RNA
Open Chromatin
Promoter
Transcription factor availability
Enhancer
RNA polymerase
Nucleosome occupancy
Cis-regulatory elements
B
PC1−PC2 plot
Group
Ctrl
IR
IR−lipro−1
Ctrl−2
Ctrl−3
Ctrl−1
IR−2
IR−3
IR−1
IR+lipro−1
IR+lipro−3
IR+lipro−2
PC2(9.5%)
PC1(63.4%)
C
Ctrl
IR
IR+Lipro-1
Genes
gene distance(kbp)
E
C57BL/6 IR-VS-ctrl_Down
Fatty acid biosynthesis
Fatty acid degradation
Biosynthesis of unsaturated fatty acids
Fatty acid metabolism
Sphingolipid metabolism
Citrate cycle (TCA cycle)
Fatty acid elongation
Arachidonic acid metabolism
Cysteine and methionine metabolism
Glutathione metabolism
Count
-log10(P-value)
Rich Factor
D
Classical ferroptosis related genes
chr13: 56,584,474-56,602,686
Slc25a48
chr2: 75,521,587-75,535,278
Nfe2l2
chr14:47,389,352-47,428,870
Gch1
Lipid metabolism related genes
chr9:46,177,906-46,185,219
Apoa5
chr19:44,380,889-44,398,148
Scd1
chr19:10,061,533-10,080,040
Fads2
sham#1
sham#2
IR#1
IR#2
IR+Lipro-1#1
IR+Lipro-1#2
1kb

Figure S2.

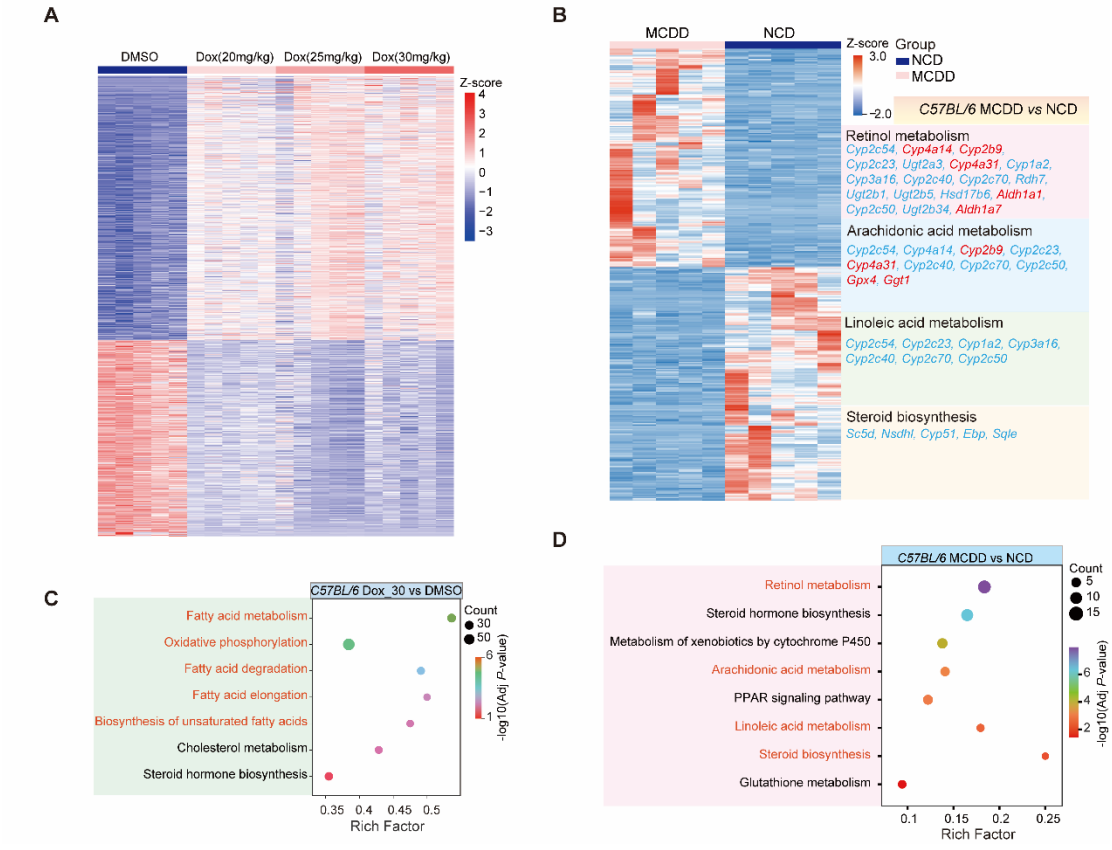
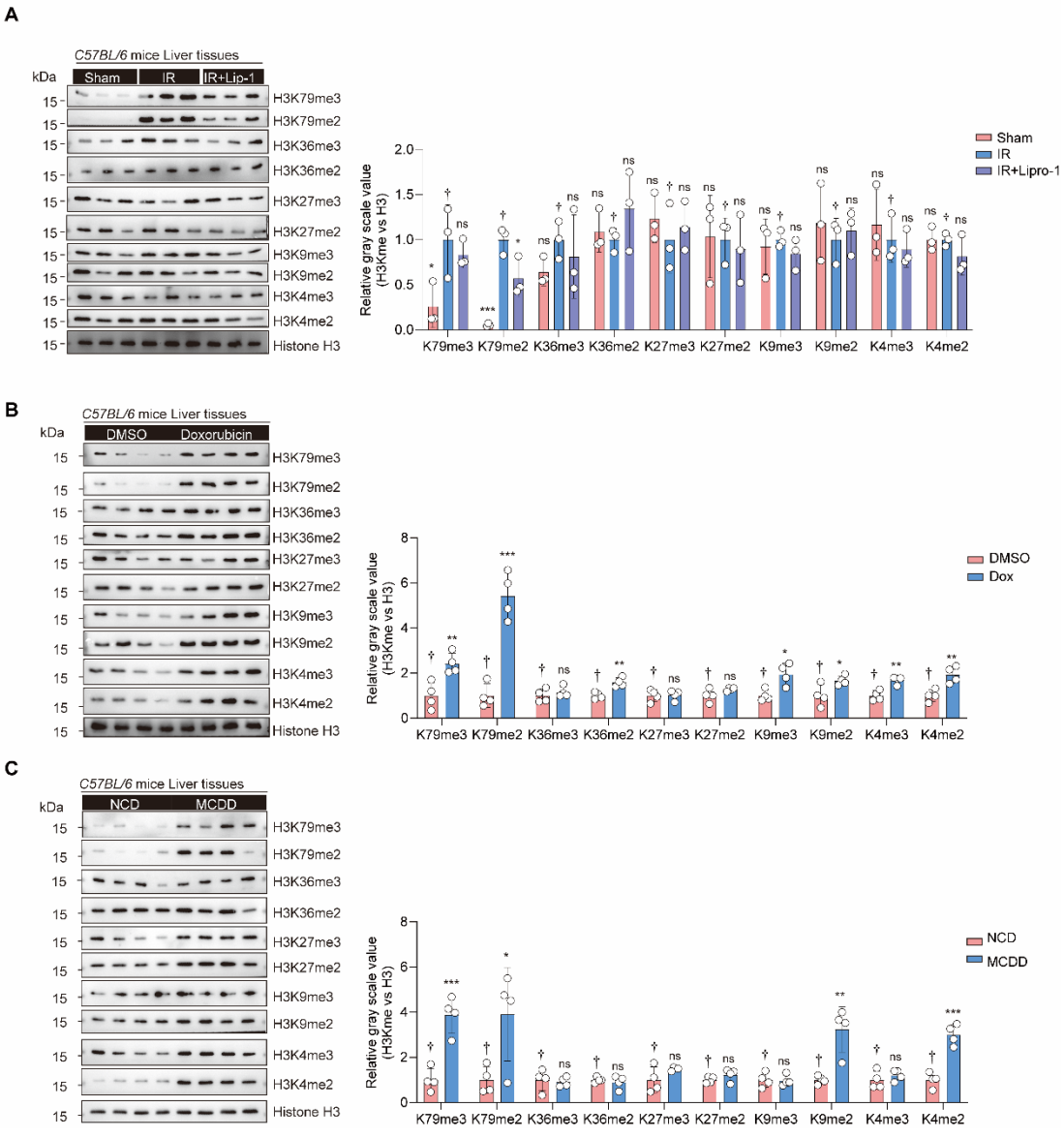

A
DMSO
Dox(20mg/kg)
Dox(25mg/kg)
Dox(30mg/kg)
Z-score
4
3
2
1
0
−1
−2
−3
B
MCDD
NCD
Z-score
3.0
−2.0
Group
NCD
MCDD
C57BL/6 MCDD vs NCD
Retinol metabolism
Cyp2c54, Cyp4a14, Cyp2b9, Cyp2c23, Ugt2a3, Cyp4a31, Cyp1a2, Cyp3a16, Cyp2c40, Cyp2c70, Rdh7, Ugt2b1, Ugt2b5, Hsd17b6, Aldh1a1, Cyp2c50, Ugt2b34, Aldh1a7
Arachidonic acid metabolism
Cyp2c54, Cyp4a14, Cyp2b9, Cyp2c23, Cyp4a31, Cyp2c40, Cyp2c70, Cyp2c50, Gpx4, Ggt1
Linoleic acid metabolism
Cyp2c54, Cyp2c23, Cyp1a2, Cyp3a16, Cyp2c40, Cyp2c70, Cyp2c50
Steroid biosynthesis
Sc5d, Nsdhl, Cyp51, Ebp, Sqle
C
C57BL/6 Dox_30 vs DMSO
Fatty acid metabolism
Oxidative phosphorylation
Fatty acid degradation
Fatty acid elongation
Biosynthesis of unsaturated fatty acids
Cholesterol metabolism
Steroid hormone biosynthesis
Count
30
50
6
1
-log10(Adj P-value)
0.35
0.4
0.45
0.5
Rich Factor
D
C57BL/6 MCDD vs NCD
Retinol metabolism
Steroid hormone biosynthesis
Metabolism of xenobiotics by cytochrome P450
Arachidonic acid metabolism
PPAR signaling pathway
Linoleic acid metabolism
Steroid biosynthesis
Glutathione metabolism
Count
5
10
15
6
4
2
-log10(Adj P-value)
0.1
0.15
0.2
0.25
Rich Factor

Figure S3.



713

Figure S4.

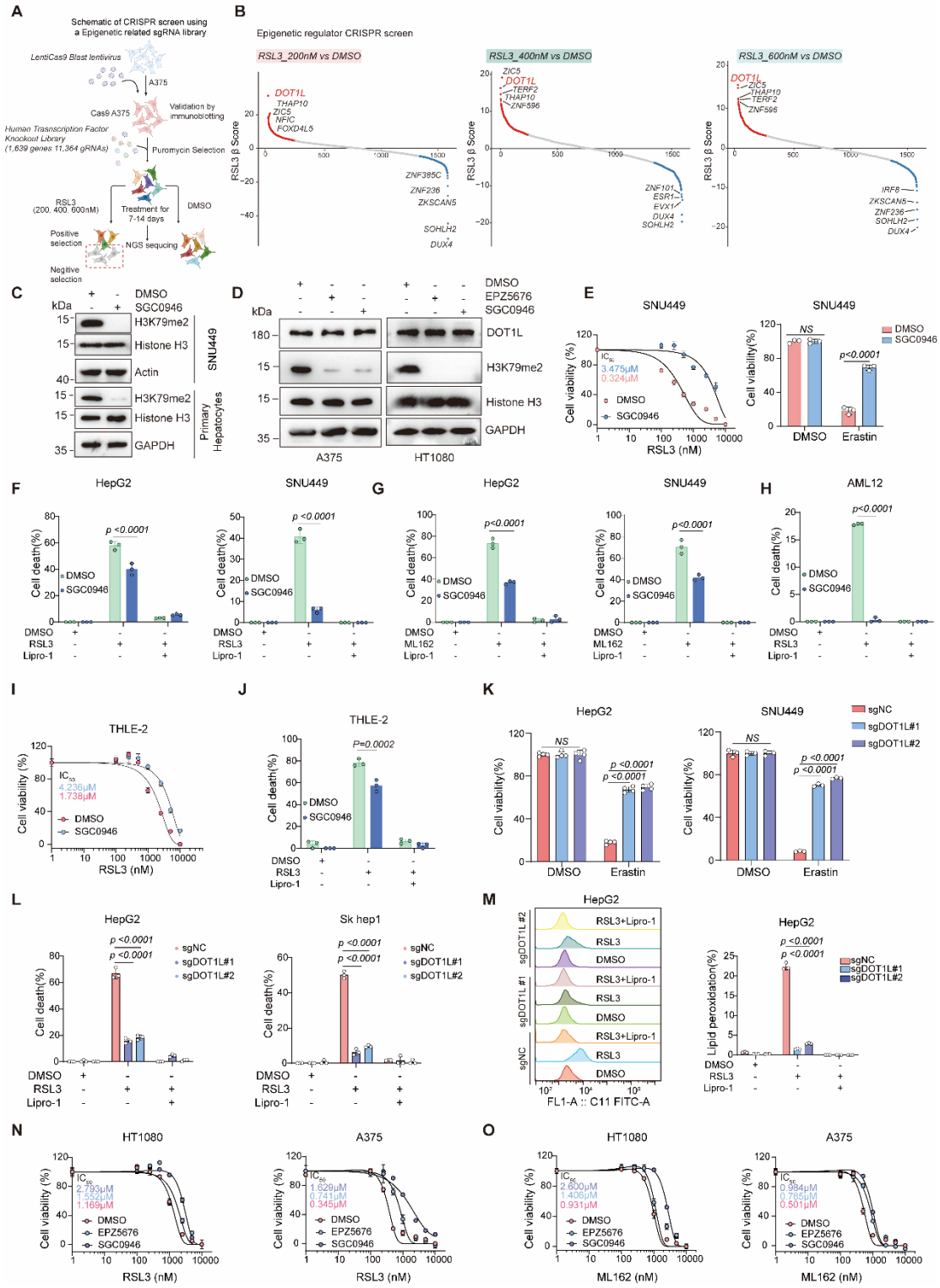

A
Schematic of CRISPR screen using a Epigenetic related sgRNA library
LentiCas9 Blast lentivirus
A375
Cas9 A375
Validation by immunoblotting
Human Trasnscription Factor Knockout Library (1,639 genes 11,364 gRNAs)
Puromycin Selection
RSL3 (200, 400, 600nM)
Treatment for 7-14 days
DMSO
Positive selection
NGS sequcing
Negative selection
B
Epigenetic regulator CRISPR screen
RSL3_200nM vs DMSO
RSL3_400nM vs DMSO
RSL3_600nM vs DMSO
RSL3 β Score
DOT1L
THAP10
ZIC5
NFIC
FOXD4L5
ZNF385C
ZNF236
ZKSCAN5
SOHLH2
DUX4
TERF2
ZNF596
ESR1
EVX1
ZNF101
IRF8
C
DMSO
SGC0946
kDa
H3K79me2
Histone H3
Actin
GAPDH
SNU449
Primary Hepatocytes
D
DMSO
EPZ5676
SGC0946
DOT1L
H3K79me2
Histone H3
GAPDH
A375
HT1080
E
SNU449
Cell viability (%)
RSL3 (nM)
IC50
3.475μM
0.324μM
DMSO
SGC0946
Erastin
NS
p<0.0001
F
HepG2
SNU449
Cell death(%)
p <0.0001
RSL3
Lipro-1
G
ML162
H
AML12
I
THLE-2
4.236μM
1.738μM
J
P=0.0002
K
sgNC
sgDOT1L#1
sgDOT1L#2
p <0.0001
L
Sk hep1
M
RSL3+Lipro-1
FL1-A :: C11 FITC-A
Lipid peroxidation(%)
N
HT1080
A375
EPZ5676
2.793μM
1.552μM
1.169μM
1.629μM
0.741μM
0.345μM
O
2.600μM
1.405μM
0.931μM
0.984μM
0.785μM
0.501μM
ML162 (nM)

Figure S5.

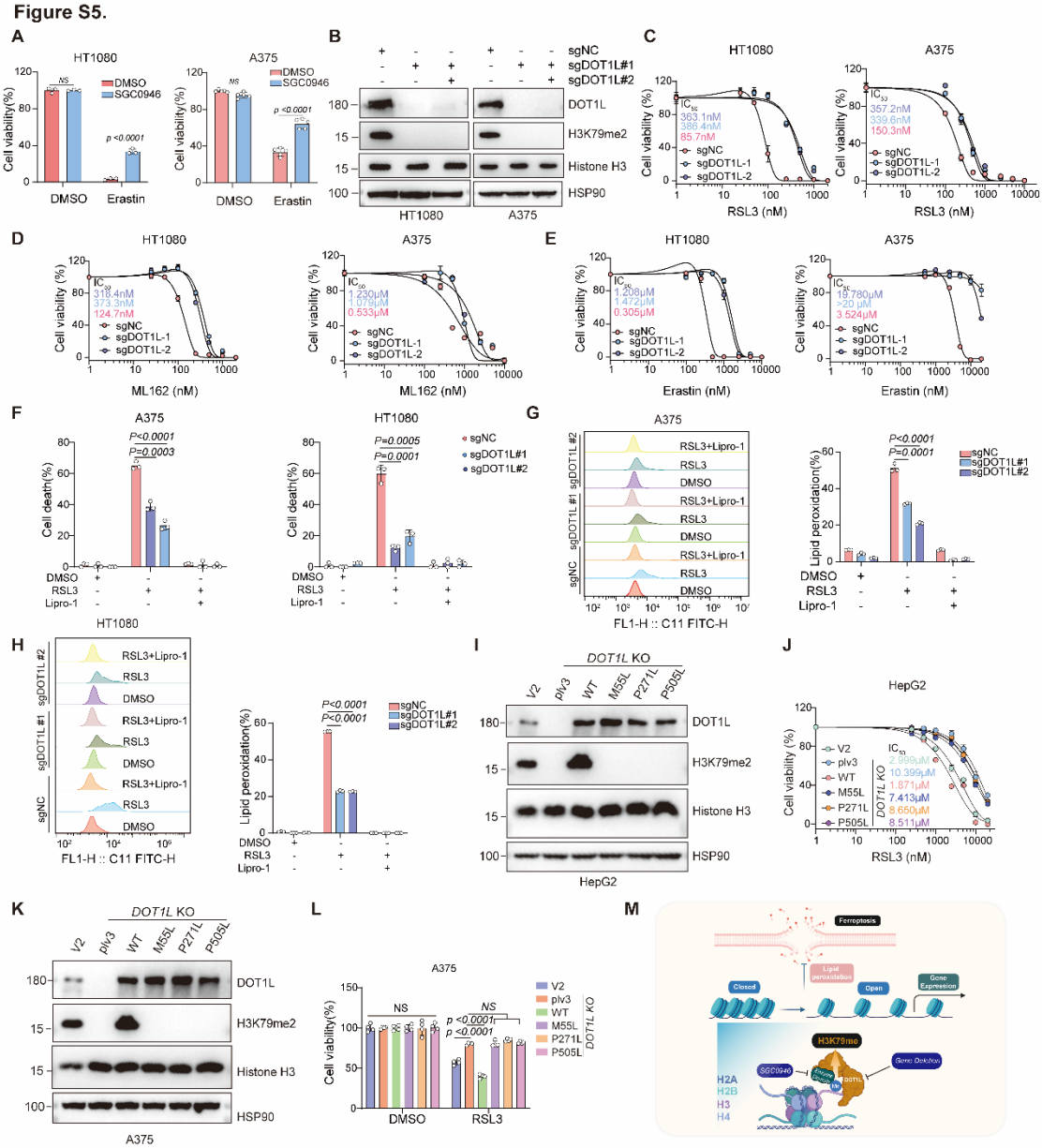

A
HT1080
A375
DMSO
SGC0946
Cell viability(%)
DMSO
Erastin
B
sgNC
sgDOT1L#1
sgDOT1L#2
DOT1L
H3K79me2
Histone H3
HSP90
HT1080
A375
C
HT1080
A375
Cell viability (%)
RSL3 (nM)
sgNC
sgDOT1L-1
sgDOT1L-2
D
HT1080
A375
ML162 (nM)
E
HT1080
A375
Erastin (nM)
F
A375
HT1080
Cell death(%)
DMSO
RSL3
Lipro-1
G
A375
RSL3+Lipro-1
RSL3
DMSO
FL1-H :: C11 FITC-H
Lipid peroxidation(%)
H
HT1080
I
DOT1L KO
V2
plv3
WT
M55L
P271L
P505L
HepG2
J
HepG2
V2
plv3
WT
M55L
P271L
P505L
DOT1L KO
K
DOT1L KO
A375
L
A375
NS
DMSO
RSL3
M
Ferroptosis
Lipid peroxidation
Closed
Open
Gene Expression
H3K79me
SGC0946
DOT1L
Gene Deletion
H2A
H2B
H3
H4

Figure S6.

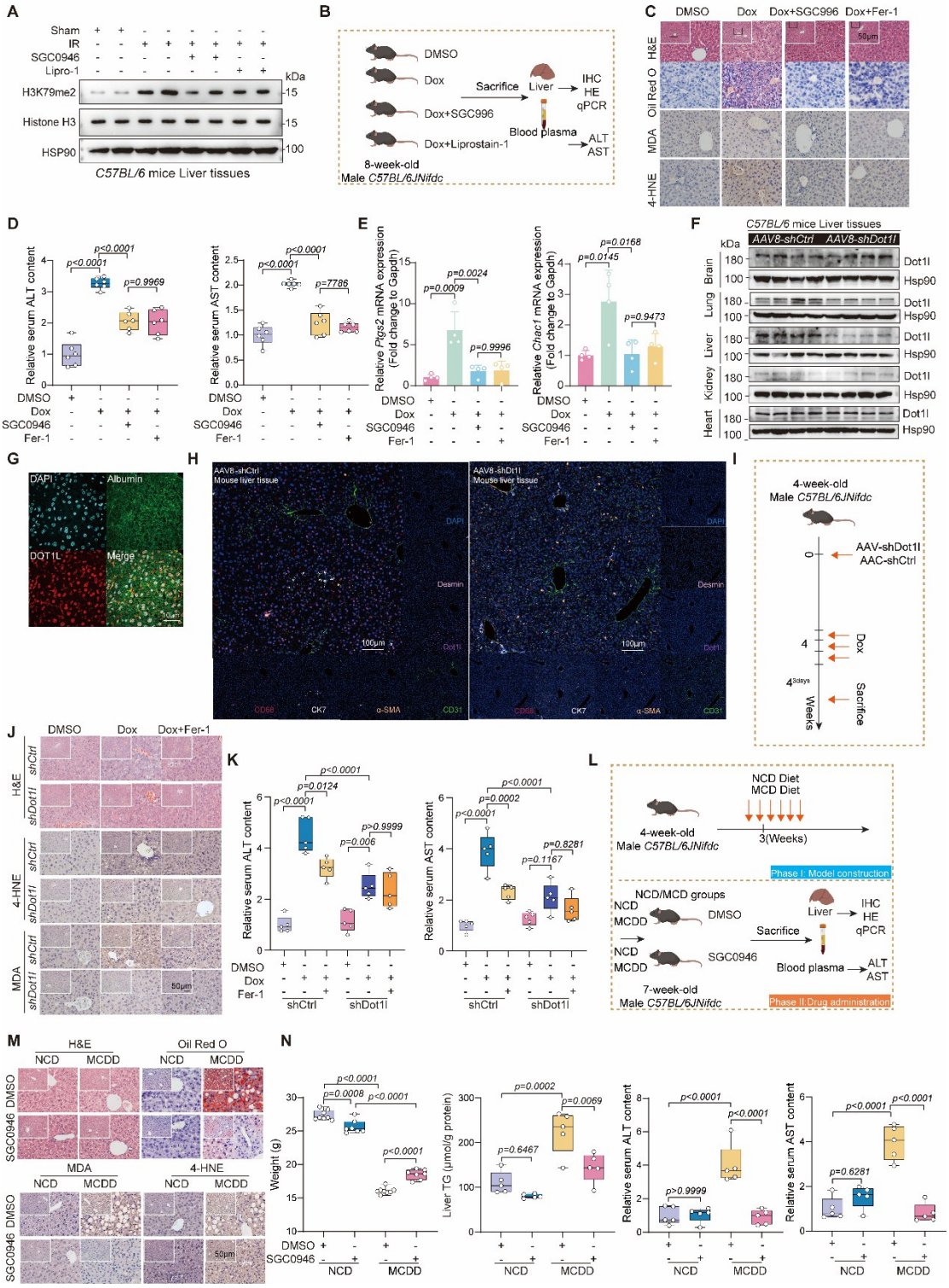

A
Sham
IR
SGC0946
Lipro-1
kDa
H3K79me2
Histone H3
HSP90
15
15
100
C57BL/6 mice Liver tissues
B
DMSO
Dox
Dox+SGC996
Dox+Liprostain-1
Sacrifice
Liver
IHC
HE
qPCR
Blood plasma
ALT
AST
8-week-old
Male C57BL/6JNifdc
C
DMSO
Dox
Dox+SGC996
Dox+Fer-1
H&E
Oil Red O
MDA
4-HNE
50μm
D
Relative serum ALT content
Relative serum AST content
p<0.0001
p=0.9969
p=7786
DMSO
Dox
SGC0946
Fer-1
E
Relative Ptgs2 mRNA expression (Fold change to Gapdh)
Relative Chac1 mRNA expression (Fold change to Gapdh)
p=0.0009
p=0.0024
p=0.9996
p=0.0145
p=0.0168
p=0.9473
F
C57BL/6 mice Liver tissues
AAV8-shCtrl
AAV8-shDot1l
kDa
Brain
Lung
Liver
Kidney
Heart
Dot1l
Hsp90
180
100
G
DAPI
Albumin
DOT1L
Merge
50μm
H
AAV8-shCtrl
Mouse liver tissue
AAV8-shDot1l
Mouse liver tissue
DAPI
Desmin
Dot1l
100μm
CD68
CK7
α-SMA
CD31
I
4-week-old
Male C57BL/6JNifdc
AAV-shDot1l
AAC-shCtrl
0
4
Dox
4days
Weeks
Sacrifice
J
DMSO
Dox
Dox+Fer-1
H&E
4-HNE
MDA
shCtrl
shDot1l
50μm
K
Relative serum ALT content
Relative serum AST content
p<0.0001
p=0.0124
p>0.9999
p=0.006
p=0.0002
p=0.8281
p=0.1167
DMSO
Dox
Fer-1
shCtrl
shDot1l
L
NCD Diet
MCD Diet
4-week-old
Male C57BL/6JNifdc
3(Weeks)
Phase I: Model construction
NCD/MCD groups
NCD
MCDD
DMSO
SGC0946
Liver
IHC
HE
qPCR
Sacrifice
Blood plasma
ALT
AST
7-week-old
Male C57BL/6JNifdc
Phase II:Drug administration
M
H&E
Oil Red O
MDA
4-HNE
NCD
MCDD
DMSO
SGC0946
50μm
N
Weight (g)
Liver TG (μmol/g protein)
Relative serum ALT content
Relative serum AST content
p<0.0001
p=0.0008
p=0.0002
p=0.0069
p=0.6467
p>0.9999
p=0.6281
DMSO
SGC0946
NCD
MCDD

Figure S7.

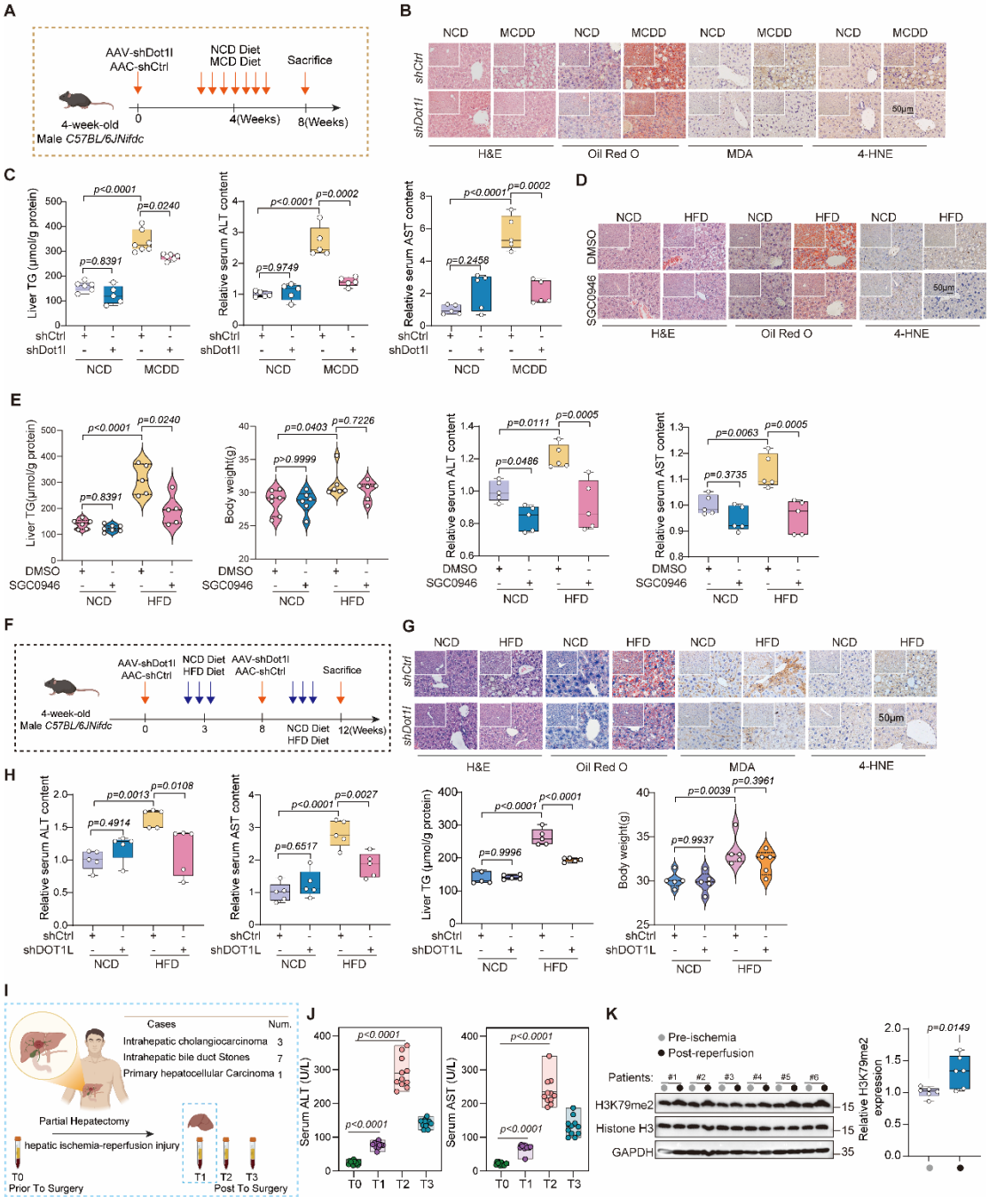

A
AAV-shDot1l
AAC-shCtrl
NCD Diet
MCD Diet
Sacrifice
4-week-old
Male C57BL/6JNifdc
0
4(Weeks)
8(Weeks)
B
NCD
MCDD
shCtrl
shDot1l
50μm
H&E
Oil Red O
MDA
4-HNE
C
Liver TG (μmol/g protein)
Relative serum ALT content
Relative serum AST content
p<0.0001
p=0.0240
p=0.8391
p=0.9749
p=0.0002
p=0.2458
shCtrl
shDot1l
NCD
MCDD
D
NCD
HFD
DMSO
SGC0946
H&E
Oil Red O
4-HNE
E
Liver TG(μmol/g protein)
Body weight(g)
Relative serum ALT content
Relative serum AST content
p=0.0403
p=0.7226
p>0.9999
p=0.0111
p=0.0005
p=0.0486
p=0.0063
p=0.3735
DMSO
SGC0946
NCD
HFD
F
AAV-shDot1l
AAC-shCtrl
NCD Diet
HFD Diet
AAV-shDot1l
AAC-shCtrl
Sacrifice
4-week-old
Male C57BL/6JNifdc
0
3
8
NCD Diet
HFD Diet
12(Weeks)
G
NCD
HFD
shCtrl
shDot1l
50μm
H&E
Oil Red O
MDA
4-HNE
H
Relative serum ALT content
Relative serum AST content
Liver TG (μmol/g protein)
Body weight(g)
p=0.0013
p=0.0108
p=0.4914
p<0.0001
p=0.0027
p=0.6517
p=0.9996
p=0.0039
p=0.3961
p=0.9937
shCtrl
shDOT1L
NCD
HFD
I
Cases
Num.
Intrahepatic cholangiocarcinoma 3
Intrahepatic bile duct Stones 7
Primary hepatocellular Carcinoma 1
Partial Hepatectomy
hepatic ischemia-reperfusion injury
T0
Prior To Surgery
T1
T2
T3
Post To Surgery
J
Serum ALT (U/L)
Serum AST (U/L)
p<0.0001
T0
T1
T2
T3
K
Pre-ischemia
Post-reperfusion
Patients:
#1
#2
#3
#4
#5
#6
H3K79me2
Histone H3
GAPDH
15
15
35
Relative H3K79me2 expression
p=0.0149

Figure S8.

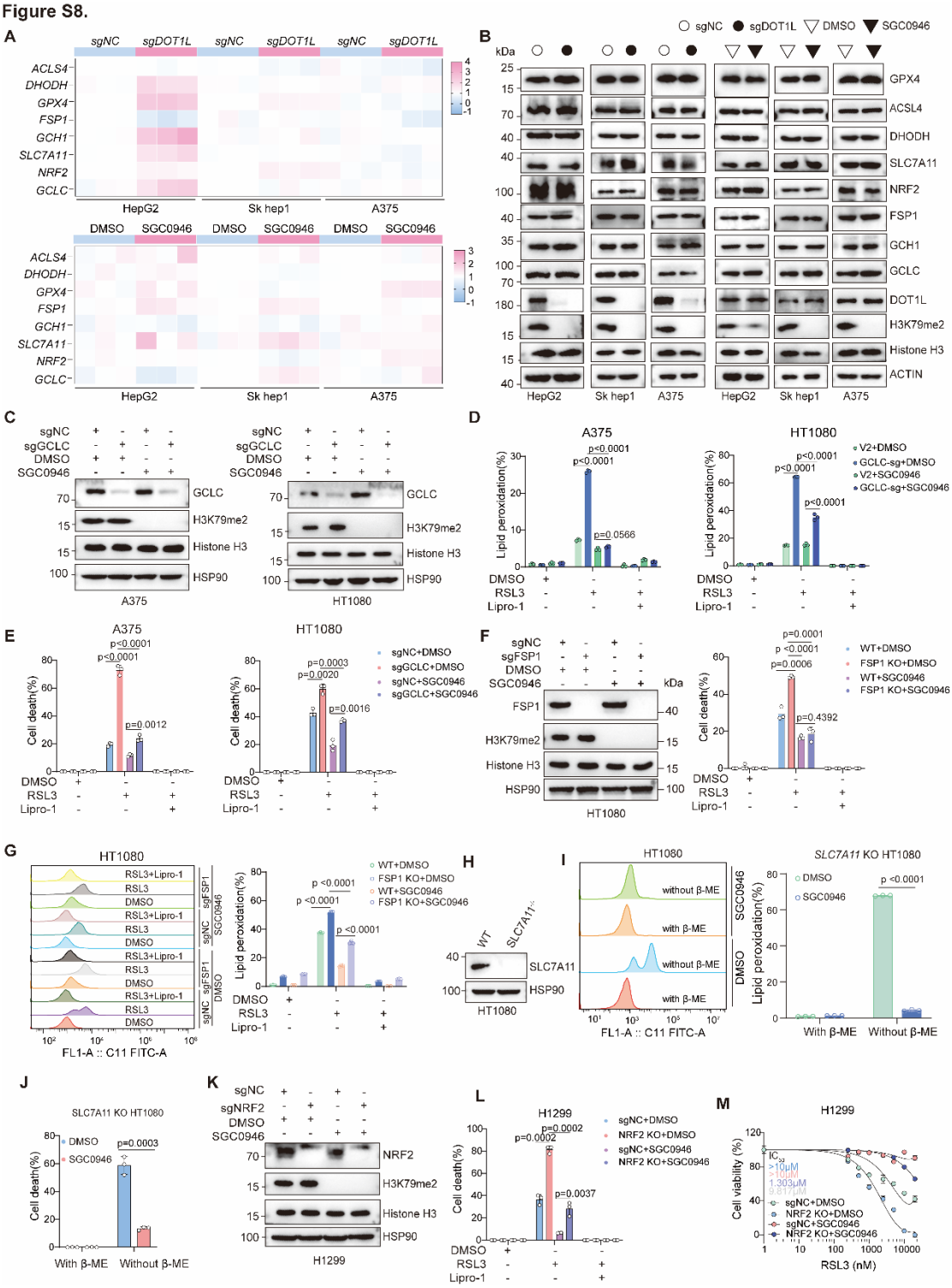

A
sgNC
sgDOT1L
ACLS4
DHODH
GPX4
FSP1
GCH1
SLC7A11
NRF2
GCLC
HepG2
Sk hep1
A375
DMSO
SGC0946
B
kDa
GPX4
ACSL4
DHODH
SLC7A11
NRF2
FSP1
GCH1
GCLC
DOT1L
H3K79me2
Histone H3
ACTIN
C
sgGCLC
GCLC
H3K79me2
Histone H3
HSP90
A375
HT1080
D
Lipid peroxidation(%)
RSL3
Lipro-1
V2+DMSO
GCLC-sg+DMSO
V2+SGC0946
GCLC-sg+SGC0946
E
Cell death(%)
sgNC+DMSO
sgGCLC+DMSO
sgNC+SGC0946
sgGCLC+SGC0946
F
sgFSP1
FSP1
WT+DMSO
FSP1 KO+DMSO
WT+SGC0946
FSP1 KO+SGC0946
G
RSL3+Lipro-1
RSL3
DMSO
FL1-A :: C11 FITC-A
H
WT
SLC7A11-/-
SLC7A11
HSP90
I
without β-ME
with β-ME
SLC7A11 KO HT1080
With β-ME
Without β-ME
J
SLC7A11 KO HT1080
K
sgNRF2
NRF2
H1299
L
NRF2 KO+DMSO
NRF2 KO+SGC0946
M
Cell viability (%)
IC50
>10μM
>10μM
1.303μM
9.817μM
RSL3 (nM)

Figure S9.

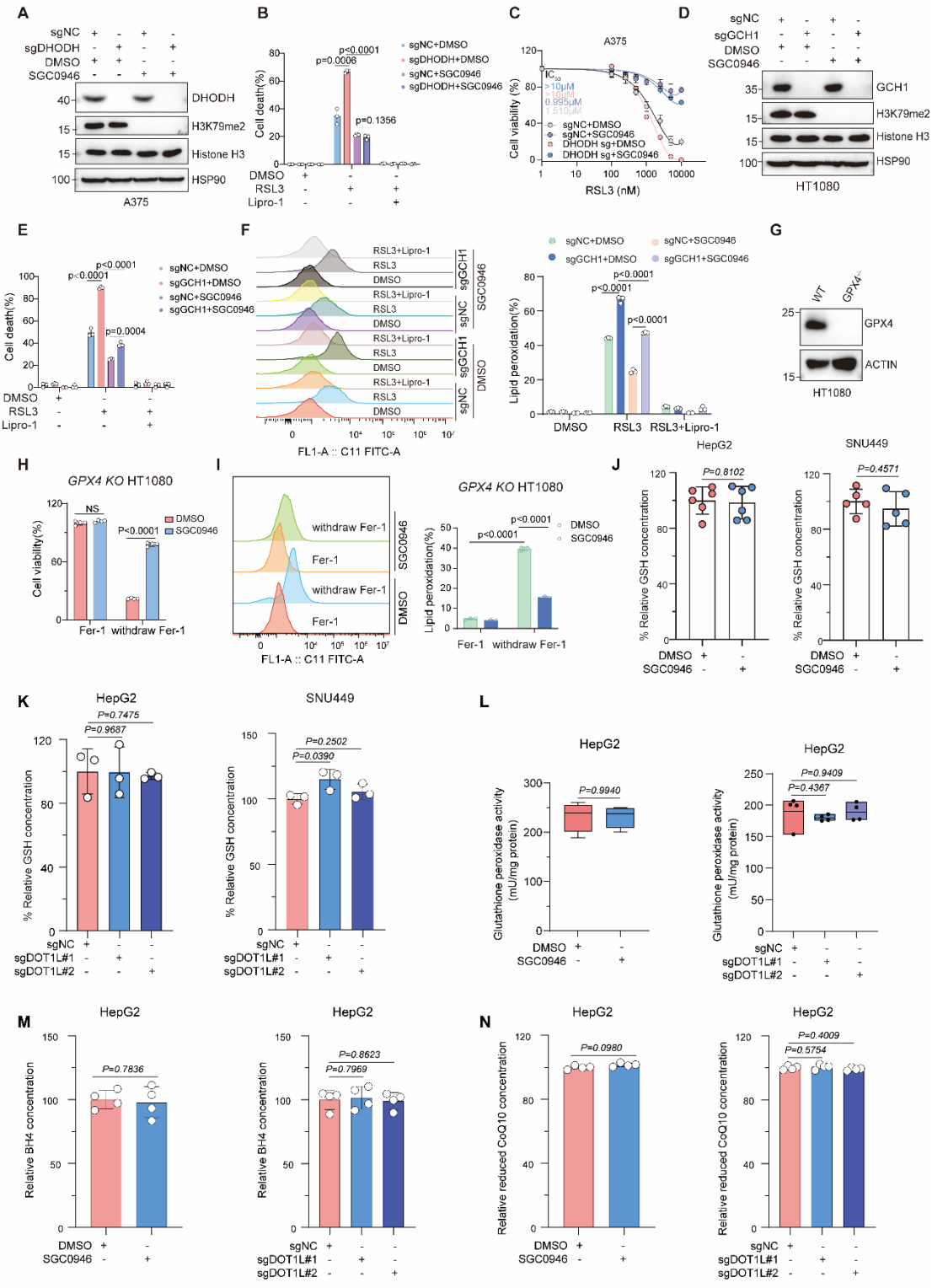

A
sgNC
sgDHODH
DMSO
SGC0946
DHODH
H3K79me2
Histone H3
HSP90
A375
B
Cell death(%)
p<0.0001
p=0.0006
p=0.1356
sgNC+DMSO
sgDHODH+DMSO
sgNC+SGC0946
sgDHODH+SGC0946
DMSO
RSL3
Lipro-1
C
A375
Cell viability (%)
IC50
>10μM
>10μM
0.995μM
1.510μM
sgNC+DMSO
sgNC+SGC0946
DHODH sg+DMSO
DHODH sg+SGC0946
RSL3 (nM)
D
sgNC
sgGCH1
DMSO
SGC0946
GCH1
H3K79me2
Histone H3
HSP90
HT1080
E
Cell death(%)
p<0.0001
p<0.0001
p=0.0004
sgNC+DMSO
sgGCH1+DMSO
sgNC+SGC0946
sgGCH1+SGC0946
DMSO
RSL3
Lipro-1
F
RSL3+Lipro-1
RSL3
DMSO
sgGCH1
sgNC
SGC0946
DMSO
FL1-A :: C11 FITC-A
sgNC+DMSO
sgNC+SGC0946
sgGCH1+DMSO
sgGCH1+SGC0946
Lipid peroxidation(%)
p<0.0001
p<0.0001
DMSO
RSL3
RSL3+Lipro-1
G
WT
GPX4-/-
GPX4
ACTIN
HT1080
H
GPX4 KO HT1080
Cell viability(%)
NS
P<0.0001
DMSO
SGC0946
Fer-1
withdraw Fer-1
I
withdraw Fer-1
Fer-1
withdraw Fer-1
Fer-1
SGC0946
DMSO
FL1-A :: C11 FITC-A
GPX4 KO HT1080
Lipid peroxidation(%)
p<0.0001
p<0.0001
DMSO
SGC0946
Fer-1
withdraw Fer-1
J
HepG2
SNU449
% Relative GSH concentration
P=0.8102
P=0.4571
DMSO
SGC0946
K
HepG2
SNU449
% Relative GSH concentration
P=0.7475
P=0.9687
P=0.2502
P=0.0390
sgNC
sgDOT1L#1
sgDOT1L#2
L
HepG2
HepG2
Glutathione peroxidase activity (mU/mg protein)
P=0.9940
P=0.9409
P=0.4367
DMSO
SGC0946
sgNC
sgDOT1L#1
sgDOT1L#2
M
HepG2
HepG2
Relative BH4 concentration
P=0.7836
P=0.8623
P=0.7969
DMSO
SGC0946
sgNC
sgDOT1L#1
sgDOT1L#2
N
HepG2
HepG2
Relative reduced CoQ10 concentration
P=0.0980
P=0.4009
P=0.5754
DMSO
SGC0946
sgNC
sgDOT1L#1
sgDOT1L#2

Figure S10.

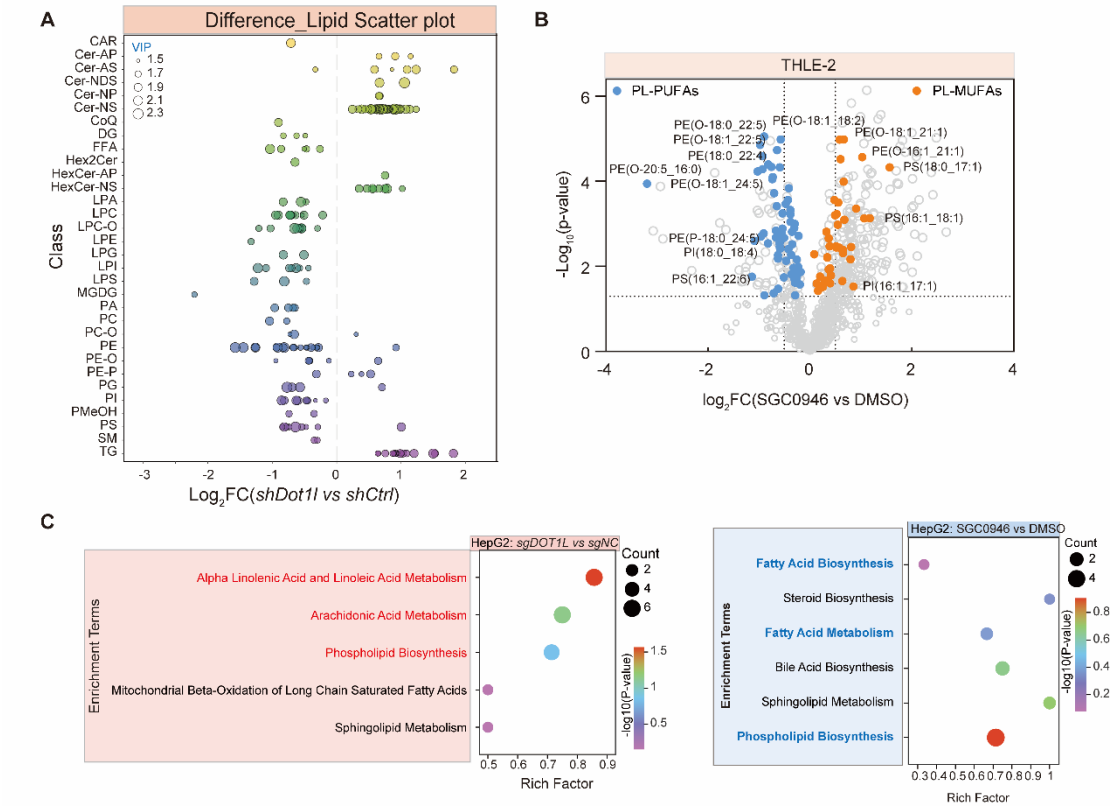

A
Difference_Lipid Scatter plot
VIP
1.5
1.7
1.9
2.1
2.3
CAR
Cer-AP
Cer-AS
Cer-NDS
Cer-NP
Cer-NS
CoQ
DG
FFA
Hex2Cer
HexCer-AP
HexCer-NS
LPA
LPC
LPC-O
LPE
LPG
LPI
LPS
MGDG
PA
PC
PC-O
PE
PE-O
PE-P
PG
PI
PMeOH
PS
SM
TG
Class
Log2FC(shDot1l vs shCtrl)
B
THLE-2
PL-PUFAs
PL-MUFAs
PE(O-18:0_22:5)
PE(O-18:1_22:5)
PE(18:0_22:4)
PE(O-20:5_16:0)
PE(O-18:1_24:5)
PE(O-18:1_18:2)
PE(O-18:1_21:1)
PE(O-16:1_21:1)
PS(18:0_17:1)
PS(16:1_18:1)
PE(P-18:0_24:5)
PI(18:0_18:4)
PS(16:1_22:6)
PI(16:1_17:1)
-Log10(p-value)
log2FC(SGC0946 vs DMSO)
C
HepG2: sgDOT1L vs sgNC
Alpha Linolenic Acid and Linoleic Acid Metabolism
Arachidonic Acid Metabolism
Phospholipid Biosynthesis
Mitochondrial Beta-Oxidation of Long Chain Saturated Fatty Acids
Sphingolipid Metabolism
Enrichment Terms
Count
-log10(P-value)
Rich Factor
HepG2: SGC0946 vs DMSO
Fatty Acid Biosynthesis
Steroid Biosynthesis
Fatty Acid Metabolism
Bile Acid Biosynthesis
Sphingolipid Metabolism
Phospholipid Biosynthesis
Enrichment Terms
Count
-log10(P-value)
Rich Factor

Figure S11.

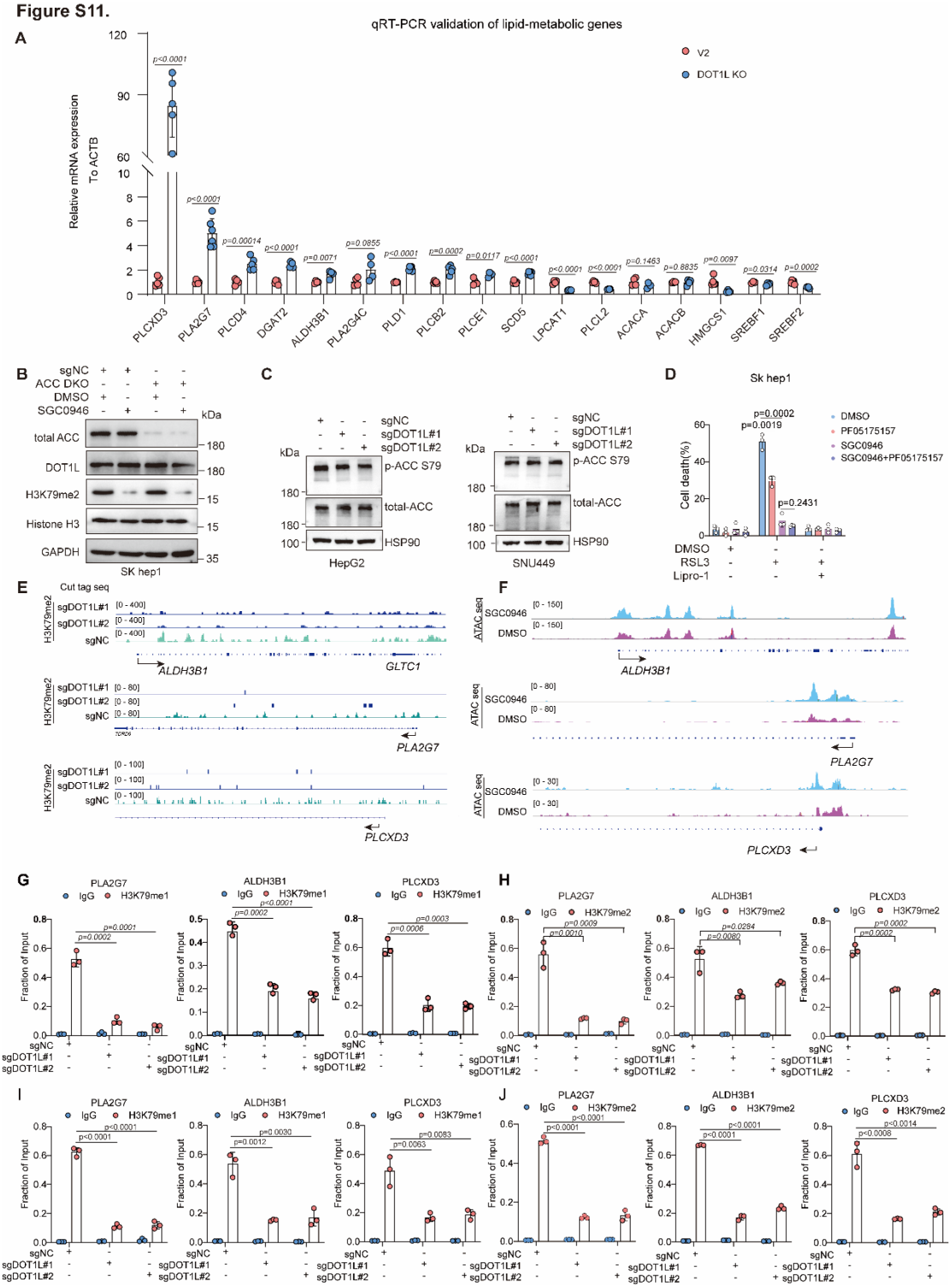

A
qRT-PCR validation of lipid-metabolic genes
V2
DOT1L KO
Relative mRNA expression
To ACTB
PLCXD3
PLA2G7
PLCD4
DGAT2
ALDH3B1
PLA2G4C
PLD1
PLCB2
PLCE1
SCD5
LPCAT1
PLCL2
ACACA
ACACB
HMGCS1
SREBF1
SREBF2
B
sgNC
ACC DKO
DMSO
SGC0946
kDa
total ACC
DOT1L
H3K79me2
Histone H3
GAPDH
SK hep1
C
sgNC
sgDOT1L#1
sgDOT1L#2
p-ACC S79
total-ACC
HSP90
HepG2
SNU449
D
Sk hep1
DMSO
PF05175157
SGC0946
SGC0946+PF05175157
Cell death(%)
DMSO
RSL3
Lipro-1
E
Cut tag seq
H3K79me2
ALDH3B1
GLTC1
PLA2G7
PLCXD3
F
ATAC seq
SGC0946
DMSO
ALDH3B1
PLA2G7
PLCXD3
G
PLA2G7
ALDH3B1
PLCXD3
IgG
H3K79me1
Fraction of Input
H
H3K79me2
I
J

Figure S12.

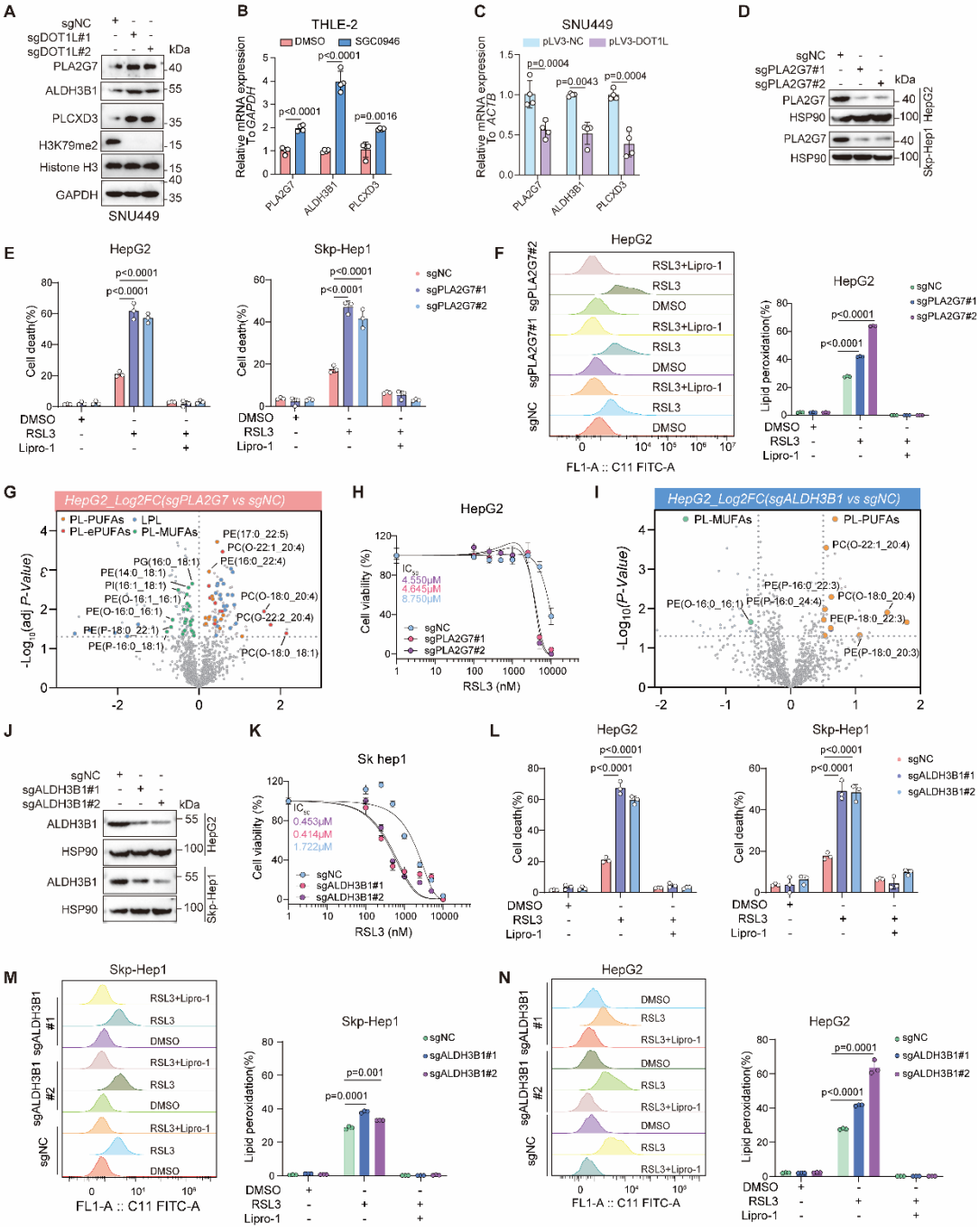

A
sgNC
sgDOT1L#1
sgDOT1L#2
kDa
PLA2G7
ALDH3B1
PLCXD3
H3K79me2
Histone H3
GAPDH
SNU449
B
THLE-2
DMSO
SGC0946
Relative mRNA expression To GAPDH
p<0.0001
p=0.0016
PLA2G7
ALDH3B1
PLCXD3
C
SNU449
pLV3-NC
pLV3-DOT1L
Relative mRNA expression To ACTB
p=0.0004
p=0.0043
p=0.0004
D
sgNC
sgPLA2G7#1
sgPLA2G7#2
HSP90
HepG2
Skp-Hep1
E
HepG2
Skp-Hep1
Cell death(%)
p<0.0001
DMSO
RSL3
Lipro-1
sgNC
sgPLA2G7#1
sgPLA2G7#2
F
HepG2
RSL3+Lipro-1
RSL3
DMSO
FL1-A :: C11 FITC-A
Lipid peroxidation(%)
G
HepG2_Log2FC(sgPLA2G7 vs sgNC)
PL-PUFAs
LPL
PL-ePUFAs
PL-MUFAs
-Log10(adj P-Value)
PE(17:0_22:5)
PC(O-22:1_20:4)
PE(16:0_22:4)
PG(16:0_18:1)
PE(14:0_18:1)
PI(16:1_18:1)
PE(O-18:1_16:1)
PC(O-18:0_20:4)
PE(O-16:0_16:1)
PC(O-22:2_20:4)
PE(P-18:0_22:1)
PE(P-16:0_18:1)
PC(O-18:0_18:1)
H
HepG2
Cell viability (%)
IC50
4.550μM
4.645μM
8.750μM
RSL3 (nM)
I
HepG2_Log2FC(sgALDH3B1 vs sgNC)
PL-MUFAs
PL-PUFAs
PC(O-22:1_20:4)
PE(P-16:0_22:3)
PE(O-16:0_16:1)
PE(P-16:0_24:4)
PC(O-18:0_20:4)
PE(P-18:0_22:3)
PE(P-18:0_20:3)
J
sgNC
sgALDH3B1#1
sgALDH3B1#2
kDa
ALDH3B1
HSP90
HepG2
Skp-Hep1
K
Sk hep1
Cell viability (%)
IC50
0.453μM
0.414μM
1.722μM
RSL3 (nM)
L
HepG2
Skp-Hep1
Cell death(%)
p<0.0001
DMSO
RSL3
Lipro-1
sgNC
sgALDH3B1#1
sgALDH3B1#2
M
Skp-Hep1
sgALDH3B1 #1
sgALDH3B1 #2
sgNC
RSL3+Lipro-1
RSL3
DMSO
FL1-A :: C11 FITC-A
Lipid peroxidation(%)
p=0.001
p=0.0001
N
HepG2
p=0.0001
p<0.0001

Figure S13.

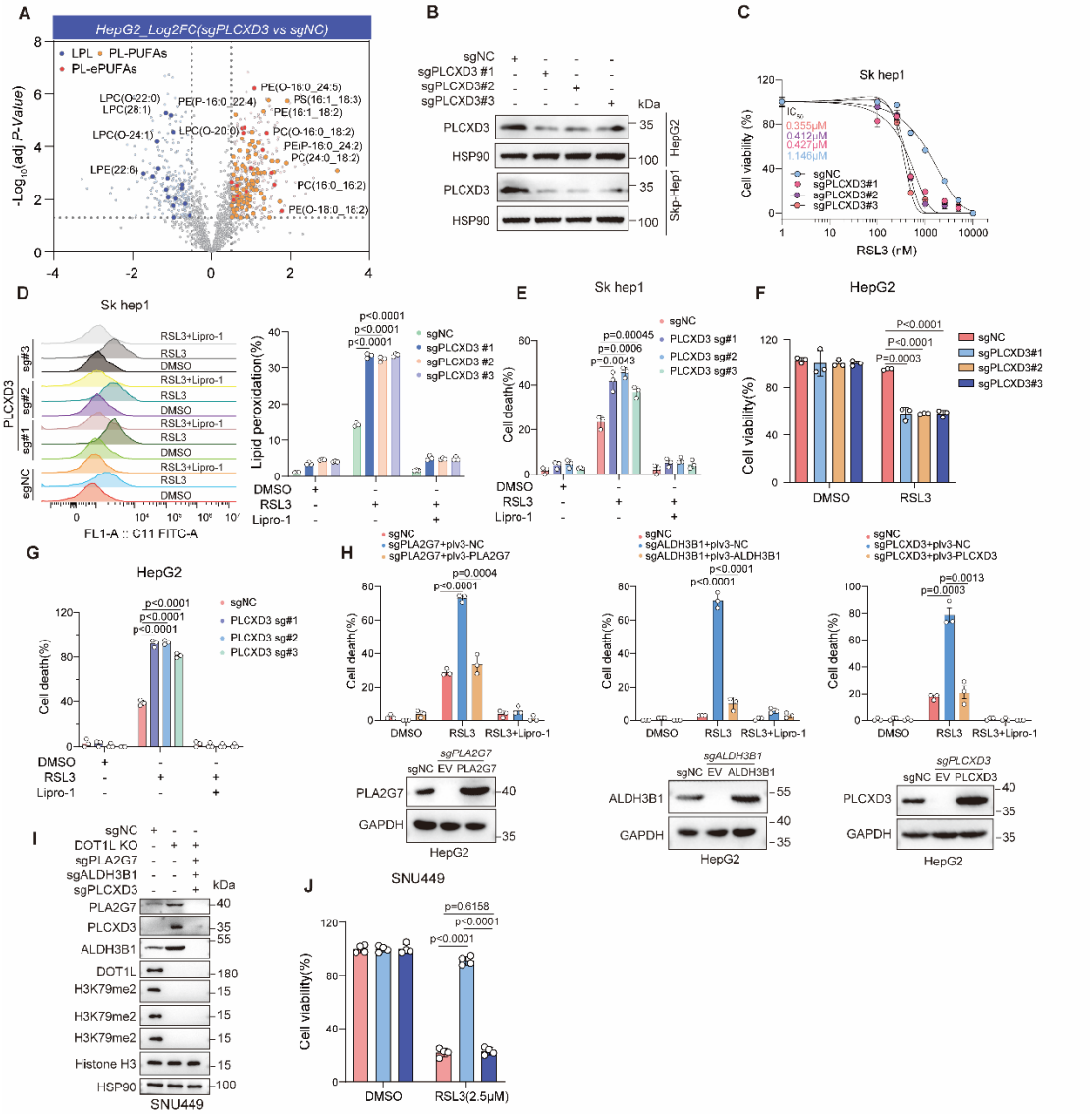

A
HepG2_Log2FC(sgPLCXD3 vs sgNC)
LPL
PL-PUFAs
PL-ePUFAs
-Log10(adj P-Value)
B
sgNC
sgPLCXD3 #1
sgPLCXD3#2
sgPLCXD3#3
kDa
PLCXD3
HSP90
HepG2
Skp-Hep1
C
Sk hep1
Cell viability (%)
RSL3 (nM)
sgNC
sgPLCXD3#1
sgPLCXD3#2
sgPLCXD3#3
D
Sk hep1
PLCXD3
RSL3+Lipro-1
RSL3
DMSO
FL1-A :: C11 FITC-A
Lipid peroxidation(%)
E
Sk hep1
Cell death(%)
PLCXD3 sg#1
PLCXD3 sg#2
PLCXD3 sg#3
F
HepG2
Cell viability(%)
G
HepG2
Cell death(%)
H
sgPLA2G7+plv3-NC
sgPLA2G7+plv3-PLA2G7
sgALDH3B1+plv3-NC
sgALDH3B1+plv3-ALDH3B1
sgPLCXD3+plv3-NC
sgPLCXD3+plv3-PLCXD3
sgPLA2G7
sgALDH3B1
sgPLCXD3
PLA2G7
ALDH3B1
GAPDH
I
sgNC
DOT1L KO
sgPLA2G7
sgALDH3B1
sgPLCXD3
PLA2G7
PLCXD3
ALDH3B1
DOT1L
H3K79me2
Histone H3
HSP90
SNU449
J
SNU449
Cell viability(%)
DMSO
RSL3(2.5μM)

Figure S14.

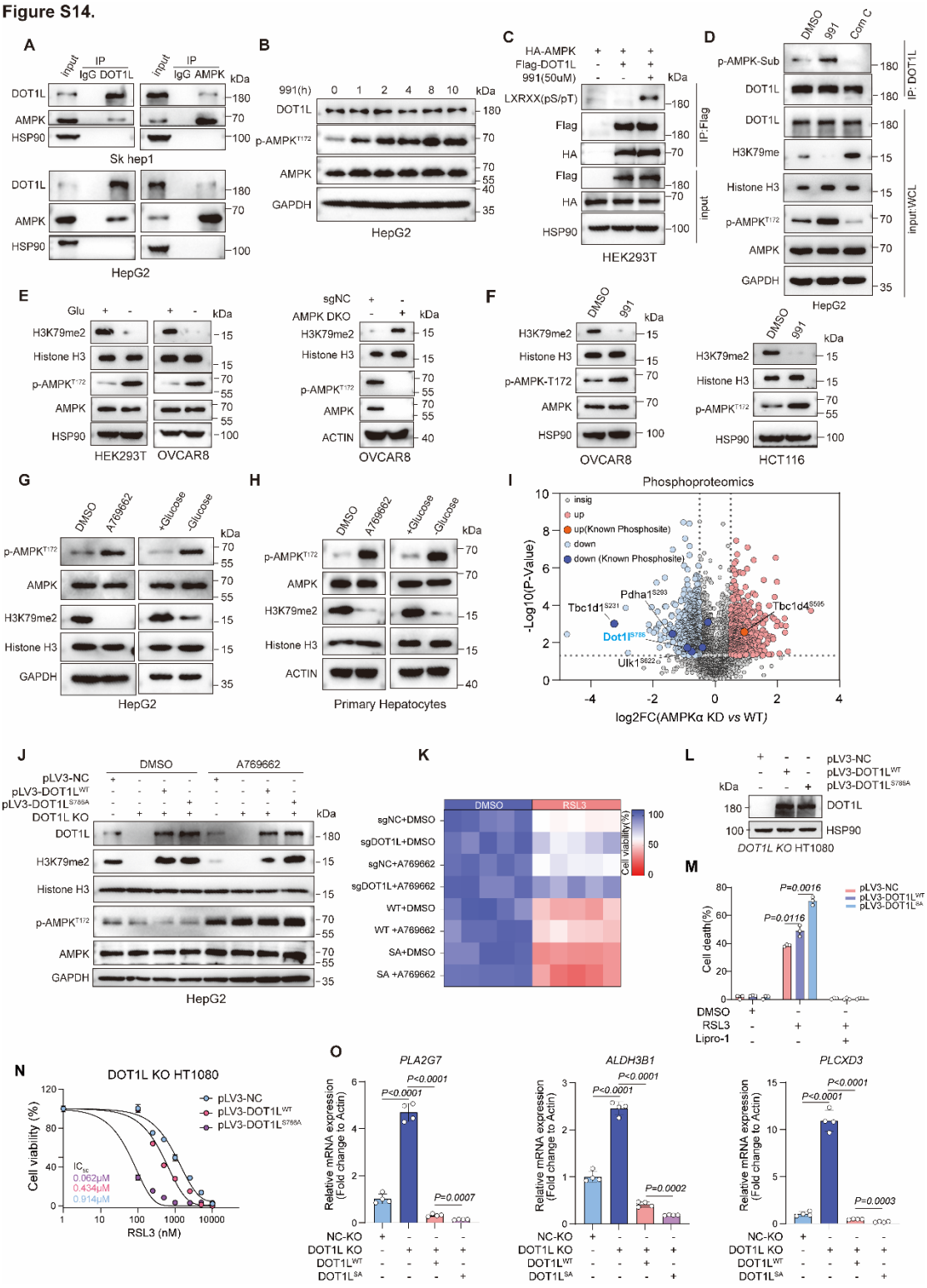

A
Input
IP IgG DOT1L
IP IgG AMPK
kDa
DOT1L
AMPK
HSP90
Sk hep1
HepG2
B
991(h) 0 1 2 4 8 10 kDa
DOT1L
p-AMPKT172
AMPK
GAPDH
HepG2
C
HA-AMPK
Flag-DOT1L
991(50uM)
LXRXX(pS/pT)
Flag
HA
HSP90
IP:Flag
input
HEK293T
D
DMSO
991
Com C
p-AMPK-Sub
DOT1L
H3K79me
Histone H3
p-AMPKT172
AMPK
GAPDH
IP: DOT1L
input:WCL
HepG2
E
Glu
H3K79me2
Histone H3
p-AMPKT172
AMPK
HSP90
HEK293T OVCAR8
sgNC
AMPK DKO
ACTIN
OVCAR8
F
DMSO
991
p-AMPK-T172
OVCAR8
HCT116
G
DMSO
A769662
+Glucose
-Glucose
HepG2
H
Primary Hepatocytes
I
Phosphoproteomics
insig
up
up(Known Phosphosite)
down
down (Known Phosphosite)
-Log10(P-Value)
log2FC(AMPKα KD vs WT)
Pdha1S293
Tbc1d1S231
Tbc1d4S595
Dot1lS785
Ulk1S622
J
pLV3-NC
pLV3-DOT1LWT
pLV3-DOT1LS785A
DOT1L KO
HepG2
K
DMSO
RSL3
sgNC+DMSO
sgDOT1L+DMSO
sgNC+A769662
sgDOT1L+A769662
WT+DMSO
WT +A769662
SA+DMSO
SA +A769662
Cell viability(%)
L
pLV3-NC
pLV3-DOT1LWT
pLV3-DOT1LS788A
DOT1L
HSP90
DOT1L KO HT1080
M
Cell death(%)
P=0.0016
P=0.0116
DMSO
RSL3
Lipro-1
N
DOT1L KO HT1080
Cell viability (%)
IC50
0.062μM
0.434μM
0.914μM
RSL3 (nM)
O
PLA2G7
ALDH3B1
PLCXD3
Relative mRNA expression (Fold change to Actin)
P<0.0001
P=0.0007
P=0.0002
P=0.0003
NC-KO
DOT1L KO
DOT1LWT
DOT1LSA

Figure S15.

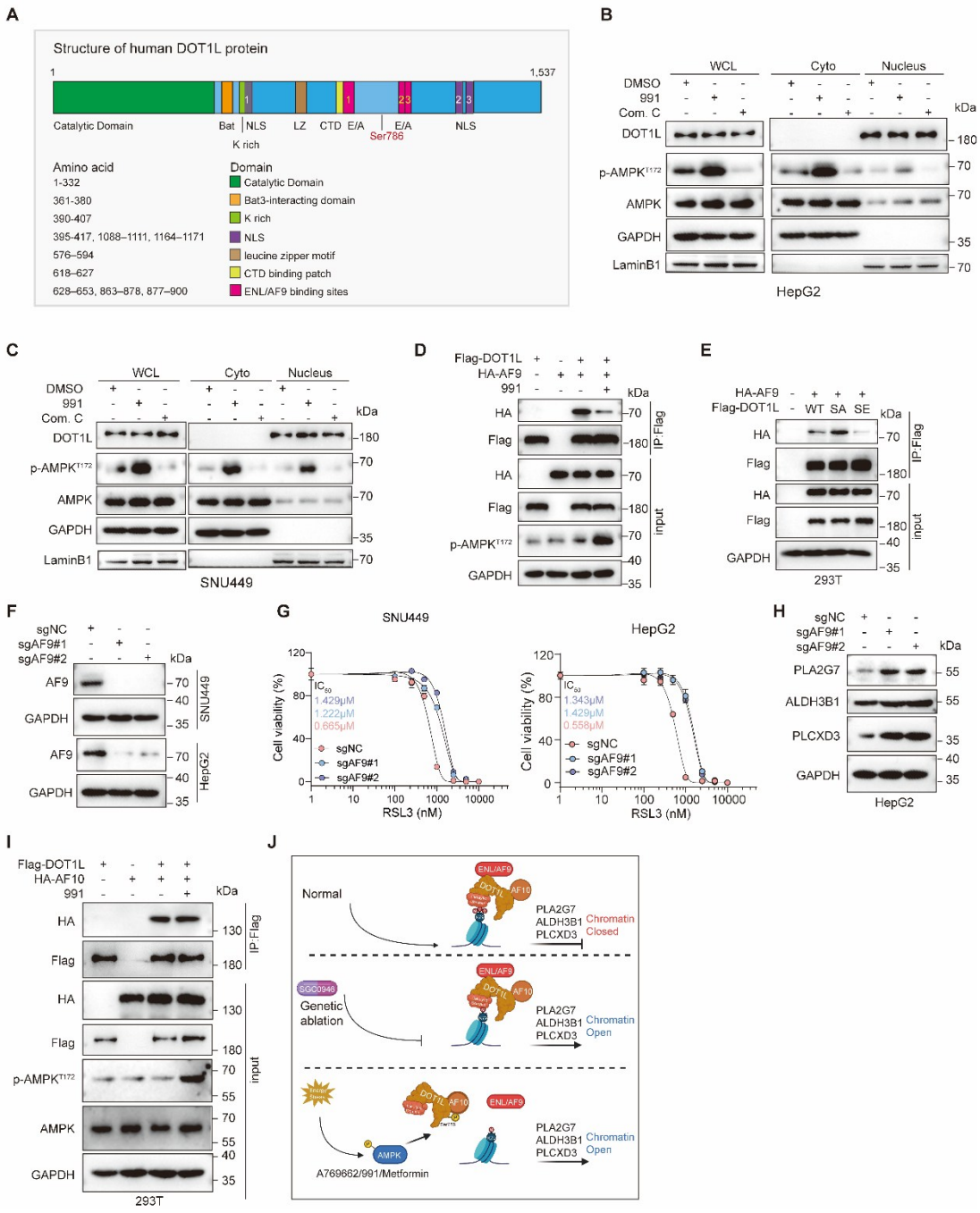

A
Structure of human DOT1L protein
1
1,537
Catalytic Domain
Bat
NLS
K rich
LZ
CTD
E/A
Ser786
E/A
NLS
Amino acid
Domain
1-332
Catalytic Domain
361-380
Bat3-interacting domain
390-407
K rich
395-417, 1088–1111, 1164–1171
NLS
576–594
leucine zipper motif
618–627
CTD binding patch
628–653, 863–878, 877–900
ENL/AF9 binding sites
B
WCL
Cyto
Nucleus
DMSO
991
Com. C
kDa
DOT1L
p-AMPKT172
AMPK
GAPDH
LaminB1
HepG2
C
SNU449
D
Flag-DOT1L
HA-AF9
991
HA
Flag
p-AMPKT172
GAPDH
IP:Flag
input
E
HA-AF9
Flag-DOT1L
WT SA SE
293T
F
sgNC
sgAF9#1
sgAF9#2
AF9
GAPDH
SNU449
HepG2
G
SNU449
HepG2
Cell viability (%)
IC50
1.429μM
1.222μM
0.685μM
1.343μM
1.429μM
0.558μM
sgNC
sgAF9#1
sgAF9#2
RSL3 (nM)
H
PLA2G7
ALDH3B1
PLCXD3
I
293T
J
Normal
ENL/AF9
DOT1L
AF10
PLA2G7
ALDH3B1
PLCXD3
Chromatin
Closed
SGC0946
Genetic ablation
Chromatin
Open
AMPK
A769662/991/Metformin

Figure S16.

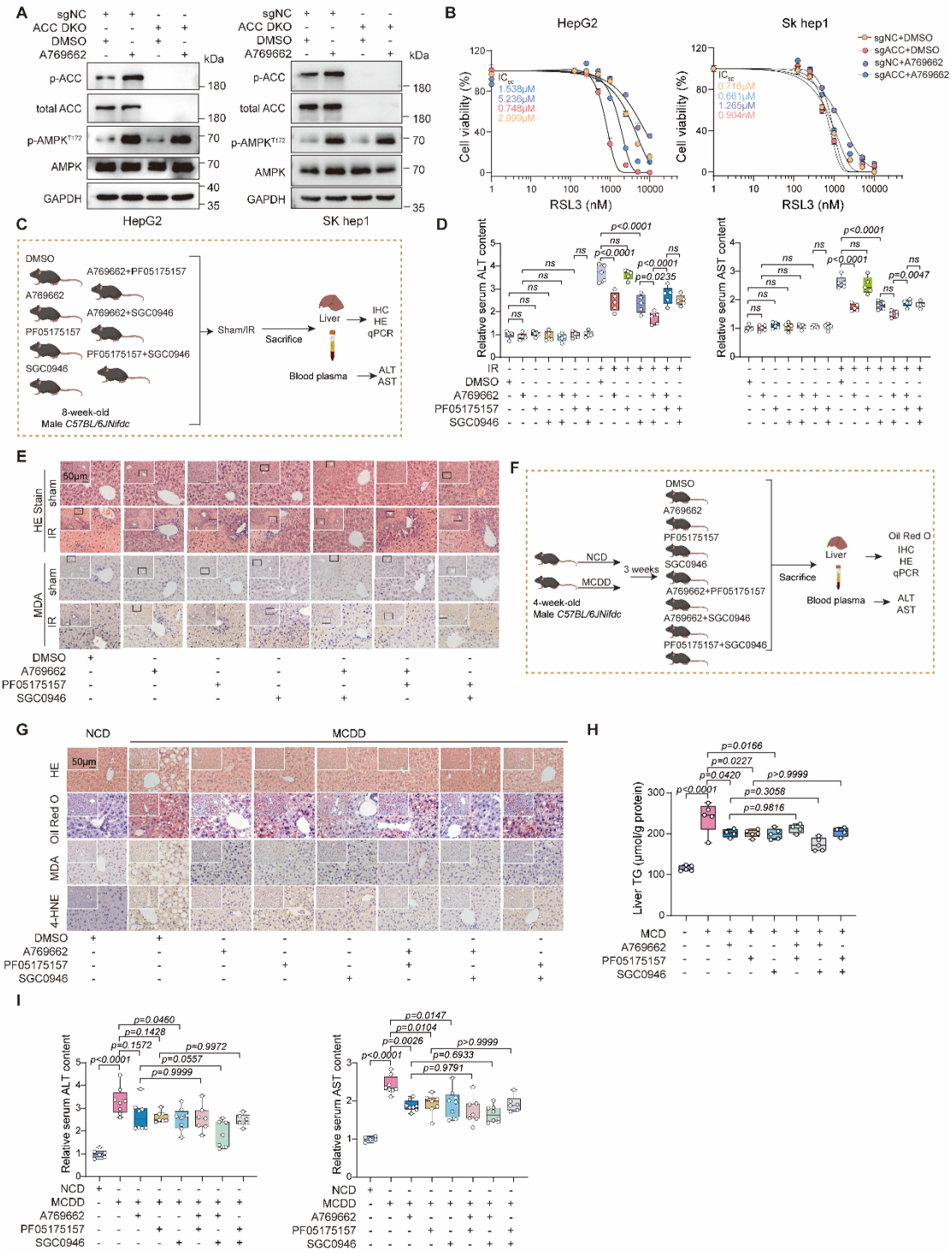

A
sgNC
ACC DKO
DMSO
A769662
kDa
p-ACC
total ACC
p-AMPK
AMPK
GAPDH
HepG2
SK hep1
B
HepG2
Sk hep1
sgNC+DMSO
sgACC+DMSO
sgNC+A769662
sgACC+A769662
Cell viability (%)
RSL3 (nM)
C
DMSO
A769662
PF05175157
SGC0946
A769662+PF05175157
A769662+SGC0946
PF05175157+SGC0946
Sham/IR
Sacrifice
Liver
Blood plasma
IHC
HE
qPCR
ALT
AST
8-week-old
Male C57BL/6JNifdc
D
Relative serum ALT content
Relative serum AST content
IR
E
HE Stain
MDA
sham
IR
50μm
F
NCD
MCDD
3 weeks
4-week-old
Male C57BL/6JNifdc
Oil Red O
G
NCD
MCDD
HE
Oil Red O
MDA
4-HNE
H
Liver TG (μmol/g protein)
I
Relative serum ALT content
Relative serum AST content

Figure S17.

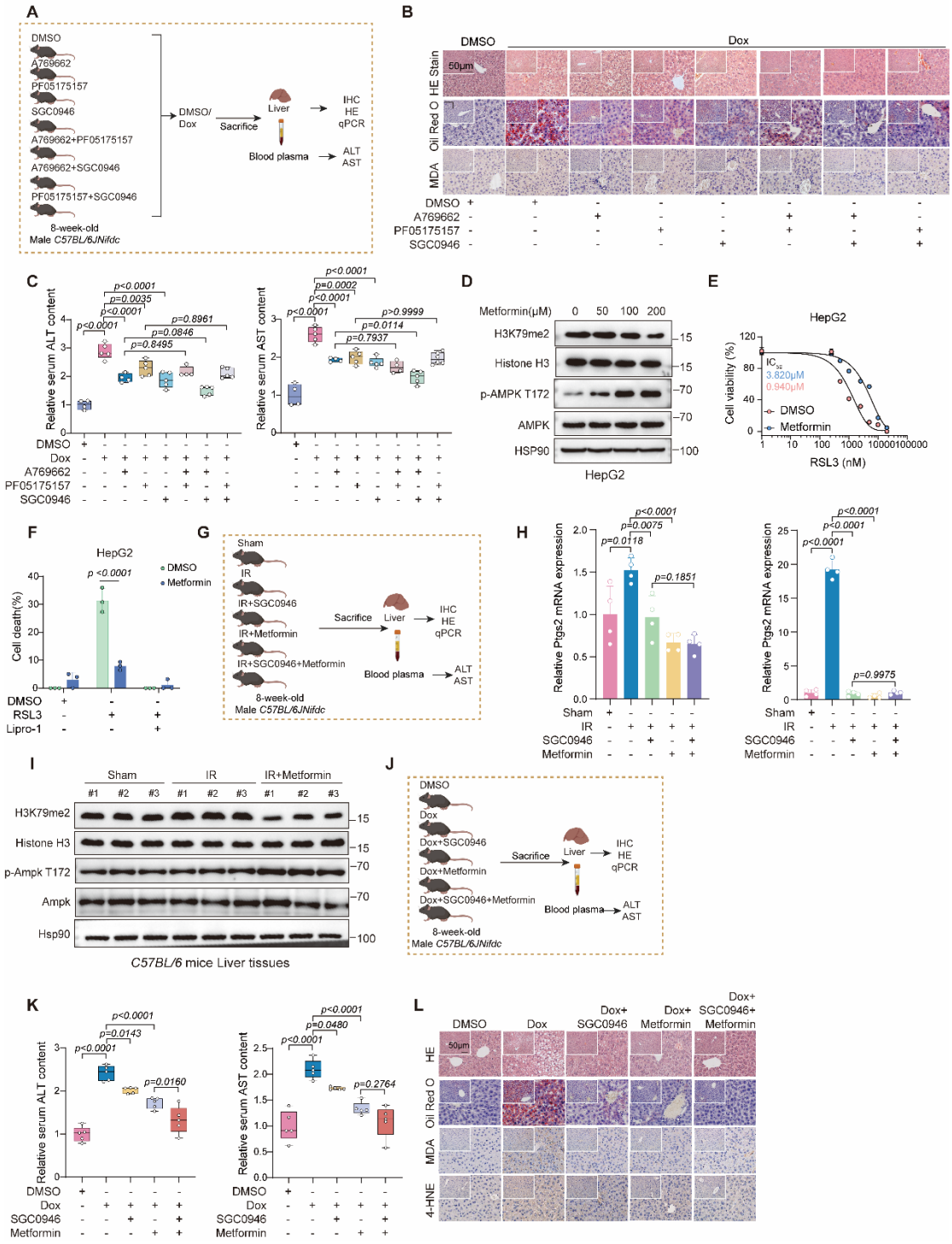

A
DMSO
A769662
PF05175157
SGC0946
A769662+PF05175157
A769662+SGC0946
PF05175157+SGC0946
8-week-old
Male C57BL/6JNifdc
DMSO/
Dox
Sacrifice
Liver
IHC
HE
qPCR
Blood plasma
ALT
AST
B
DMSO
Dox
HE Stain
Oil Red O
MDA
50μm
C
Relative serum ALT content
Relative serum AST content
D
Metformin(μM) 0 50 100 200
H3K79me2
Histone H3
p-AMPK T172
AMPK
HSP90
HepG2
E
HepG2
Cell viability (%)
IC50
3.820μM
0.940μM
DMSO
Metformin
RSL3 (nM)
F
HepG2
Cell death(%)
DMSO
Metformin
RSL3
Lipro-1
G
Sham
IR
IR+SGC0946
IR+Metformin
IR+SGC0946+Metformin
8-week-old
Male C57BL/6JNifdc
H
Relative Ptgs2 mRNA expression
Sham
IR
SGC0946
Metformin
I
Sham
IR
IR+Metformin
H3K79me2
Histone H3
p-Ampk T172
Ampk
Hsp90
C57BL/6 mice Liver tissues
J
DMSO
Dox
Dox+SGC0946
Dox+Metformin
Dox+SGC0946+Metformin
8-week-old
Male C57BL/6JNifdc
K
Relative serum ALT content
Relative serum AST content
L
DMSO
Dox
Dox+ SGC0946
Dox+ Metformin
Dox+ SGC0946+ Metformin
HE
Oil Red O
MDA
4-HNE
50μm

Figure S18.

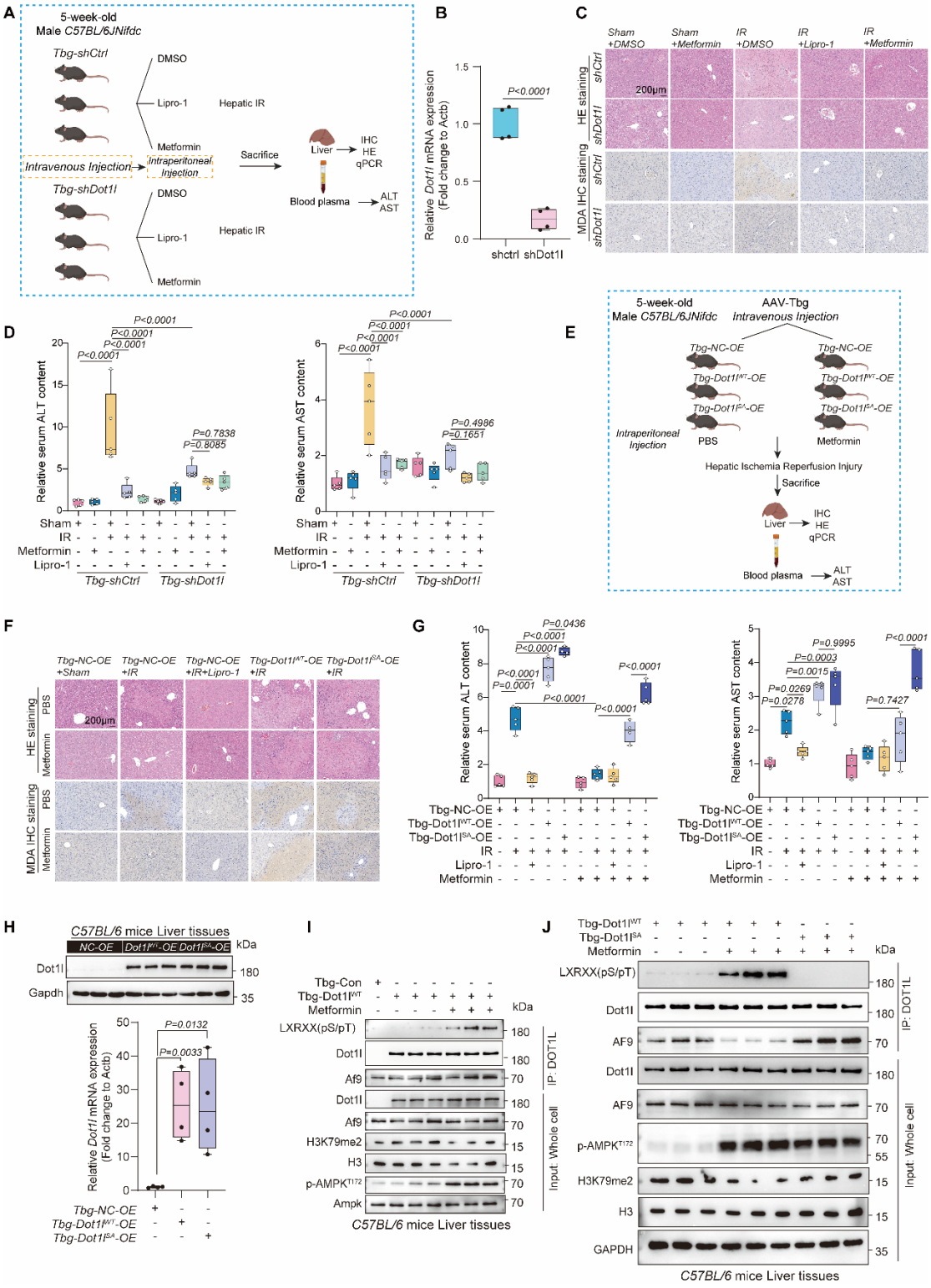
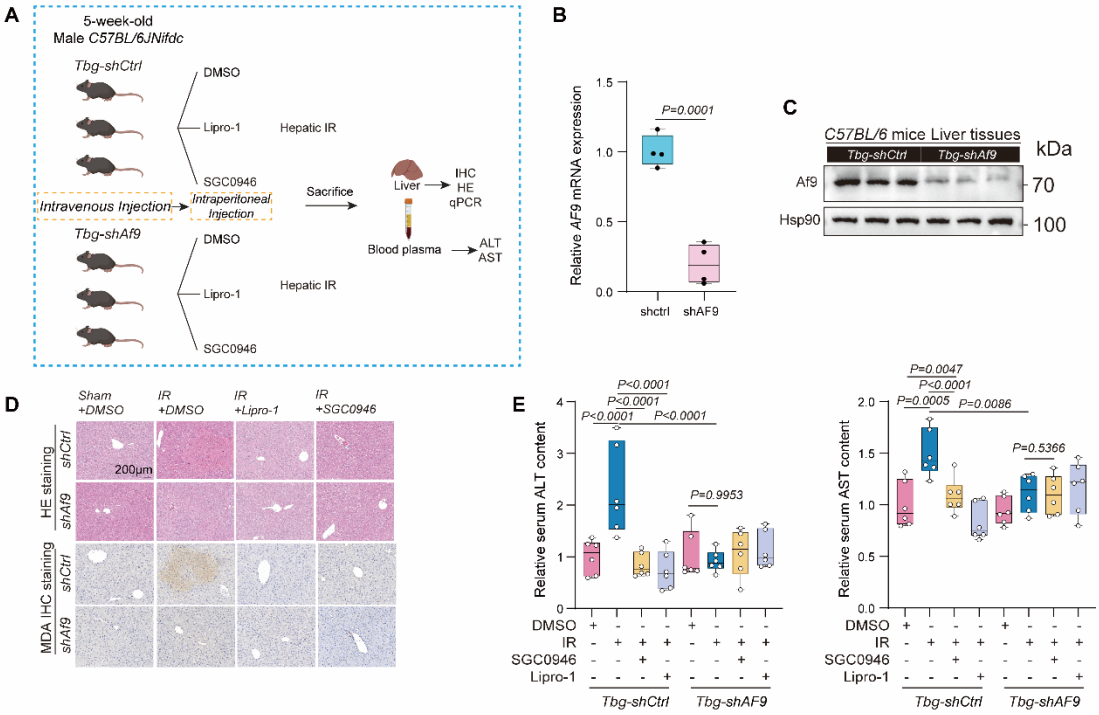

A
5-week-old
Male C57BL/6JNifdc
Tbg-shCtrl
DMSO
Lipro-1
Metformin
Hepatic IR
Intravenous Injection
Intraperitoneal Injection
Sacrifice
Liver
IHC
HE
qPCR
Blood plasma
ALT
AST
Tbg-shDot1l
B
Relative Dot1l mRNA expression (Fold change to Actb)
P<0.0001
shctrl
shDot1l
C
Sham +DMSO
Sham +Metformin
IR +DMSO
IR +Lipro-1
IR +Metformin
HE staining
MDA IHC staining
shCtrl
shDot1l
200μm
D
Relative serum ALT content
Relative serum AST content
P<0.0001
P=0.7838
P=0.8085
P=0.4986
P=0.1651
Sham
IR
Metformin
Lipro-1
Tbg-shCtrl
Tbg-shDot1l
E
5-week-old
Male C57BL/6JNifdc
AAV-Tbg
Intravenous Injection
Tbg-NC-OE
Tbg-Dot1l^WT-OE
Tbg-Dot1l^SA-OE
Intraperitoneal Injection
PBS
Metformin
Hepatic Ischemia Reperfusion Injury
Sacrifice
Liver
IHC
HE
qPCR
Blood plasma
ALT
AST
F
Tbg-NC-OE +Sham
Tbg-NC-OE +IR
Tbg-NC-OE +IR+Lipro-1
Tbg-Dot1l^WT-OE +IR
Tbg-Dot1l^SA-OE +IR
HE staining
MDA IHC staining
PBS
Metformin
200μm
G
Relative serum ALT content
Relative serum AST content
P=0.0436
P<0.0001
P=0.0001
P=0.9995
P=0.0003
P=0.0015
P=0.0269
P=0.0278
P=0.7427
Tbg-NC-OE
Tbg-Dot1l^WT-OE
Tbg-Dot1l^SA-OE
IR
Lipro-1
Metformin
H
C57BL/6 mice Liver tissues
NC-OE
Dot1l^WT-OE
Dot1l^SA-OE
kDa
Dot1l
Gapdh
180
35
Relative Dot1l mRNA expression (Fold change to Actb)
P=0.0132
P=0.0033
Tbg-NC-OE
Tbg-Dot1l^WT-OE
Tbg-Dot1l^SA-OE
I
Tbg-Con
Tbg-Dot1l^WT
Metformin
kDa
LXRXX(pS/pT)
Dot1l
Af9
H3K79me2
H3
p-AMPK^T172
Ampk
IP: DOT1L
Input: Whole cell
C57BL/6 mice Liver tissues
J
Tbg-Dot1l^WT
Tbg-Dot1l^SA
Metformin
kDa
LXRXX(pS/pT)
Dot1l
AF9
p-AMPK^T172
H3K79me2
H3
GAPDH
IP: DOT1L
Input: Whole cell
C57BL/6 mice Liver tissues

Figure S19.



729